Natural Resources Science Faculty Publications

Natural Resources Science

2020

Stream Solutes and Particulates Export Regimes: A New Framework to Optimize Their Monitoring

Florentina Moatar

Mathieu Floury

Arthur Gold
University of Rhode Island, agold@uri.edu

Michel Meybeck

Benjamin Renard

See next page for additional authors

Stream Solutes and Particulates Export Regimes: A New Framework to Optimize Their Monitoring

Creative Commons License

Authors

Florentina Moatar, Mathieu Floury, Arthur Gold, Michel Meybeck, Benjamin Renard, Martial Ferréol, André Chandesris, Camille Minaudo, Kelly Addy, Jérémy Piffady, and Gilles Pinay

Creative Commons License

Stream Solutes and Particulates Export Regimes: A New Framework to Optimize Their Monitoring

Florentina Moatar[1,2]*, Mathieu Floury[1], Arthur J. Gold[3], Michel Meybeck[4], Benjamin Renard[1], Martial Ferréol[1], André Chandesris[1], Camille Minaudo[2,5], Kelly Addy[3], Jérémy Piffady[1] and Gilles Pinay[1]

[1] INRAE, RiverLy, Villeurbanne, France, [2] University of Tours, EA 6293 GEHCO, Tours, France, [3] Department of Natural Resources Science, University of Rhode Island, Kingston, RI, United States, [4] METIS, University Paris VI, Paris, France, [5] EPFL, Physics of Aquatic Systems Laboratory, Lausanne, Switzerland

The quantification of solute and sediment export from drainage basins is challenging. A large proportion of annual or decadal loads of most constituents is exported during relatively short periods of time, a "hot moment," which vary between constituents and catchments. We developed a new framework based on concentration-discharge (C-Q) relationship to characterize the export regime of stream particulates and solutes during high water periods when the majority of annual and inter-annual load is transported. We evaluated the load flashiness index (percentage of cumulative load that occurs during the highest 2% of daily load, M_2), a function of flow flashiness (percentage of cumulative Q during the highest 2% of daily Q, W_2), and export pattern (slope of the logC-logQ relationship for Q higher than the daily median Q, b_{50high}). We established this relationship based on long-term water quality and discharge datasets of 580 streams sites of France and USA, corresponding to 2,507 concentration time series of total suspended sediments (TSS), total dissolved solutes (TDS), total phosphorus (TP), nitrate (NO_3), and dissolved organic carbon (DOC), generating 1.5 million data points in highly diverse geologic, climatic, and anthropogenic contexts. Load flashiness (M_2) increased with b_{50high} and/or W_2. Also, M_2 varied as a function of the constituent transported. M_2 had the highest values for TSS and decreased for the other constituents in the following order: TP, DOC, NO_3, TDS. Based on these results, we constructed a load-flashiness diagram to determine optimal monitoring frequency of dissolved or particulate constituents as a function of b_{50high} and W_2. Based on M_2, optimal temporal monitoring frequency of the studied constituents decreases in the following order: TSS, TP, DOC, NO_3, and TDS. Finally, we analyzed relationships between these metrics and catchments characteristics. Depending on the constituent, we explained between 30 and 40% of their M_2 variance with simple catchment characteristics, such as stream network density or percentage of intensive agriculture. Therefore, catchment characteristics can be used as a first approach to set up water quality monitoring design where no hydrological and/or water quality monitoring exist.

Keywords: water quality, nutrients, carbon, fluxes, concentration-discharge relationship

INTRODUCTION

Quantifying solute and sediment export from drainage basins is important to understanding stream biogeochemical processes (Jarvie et al., 2018), soil erosion (Vanmaercke et al., 2011), chemical weathering rates (Meybeck, 1987; Gaillardet et al., 1999), and water quality issues, such as eutrophication of inland and coastal waters (Le Moal et al., 2019) or coastal anoxia (Breitburg et al., 2018). Moreover, a reliable assessment of temporal variability of solutes and sediments transported by streams is of ecological importance for preservation and restoration of aquatic ecosystems (Scheffer et al., 2009). Also, there are socio-economic implications for flood protection and water supply management (Nemery et al., 2013).

Although solute and sediment export are related to climate, lithology, landscape structure, and land use (Burt and Pinay, 2005; Gall et al., 2013; Musolff et al., 2015; Van Meter et al., 2017), a large proportion of the annual or decadal load of sediment, particulate contaminants and even some solutes are exported during relatively short hydrological events (Syvitski and Morehead, 1999). For instance, Meybeck et al. (2003) showed that large sediment loads often occur over short periods of time, e.g., hours to days, leading to skewed distributions of suspended sediment daily loads. As total phosphorus (TP) is largely transported in particulate form, its load distribution is often skewed compared to discharge (Johnes, 2007; Minaudo et al., 2017). Up to 80% of annual dissolved organic carbon export can occur within hours to days during some extreme precipitation events (Raymond and Saiers, 2010; Yoon and Raymond, 2012). Annual export of other soluble constituents respond differently to large events. For example, a substantial portion of annual phosphate export is also associated with large events while nitrate tends to present a more uniform flux regime (Frazar et al., 2019).

Despite these findings, the European Union's Water Framework Directive and other monitoring programs worldwide continue to recommend monthly sampling for most water quality monitoring, a timeframe often not suitable to accurately quantify loads or detect temporal trends (Skeffington et al., 2015). We argue for the development of monitoring programs designed to capture, at high temporal frequency, the pulsed delivery of multiple solutes and particulates from watersheds to support robust decision making. Different indicators have been proposed, and many studies have investigated the relationship between discharge and load to characterize the temporal variability of the load delivered to streams and rivers. For instance, Meybeck et al. (2003) proposed a typological description of sediment transport at global scales using indicators based on flow duration curves and sediment loads. Using a cumulative load duration curve, where values are ranked from highest to lowest, Moatar and Meybeck (2007) and Moatar et al. (2013) introduced a metric of inequality during the highest discharge and load events.

These methods require long-term, high frequency discharge and constituent data, which are very rare.

Analysis of the concentration (C) vs. river flow (Q), or C-Q relationship, is commonly used to estimate missing concentration values in discrete surveys, particularly for load calculations (Ferguson, 1986; Crowder et al., 2007; Hirsch et al., 2010). These C-Q relationships can also decipher the biogeochemical processes and the spatial dynamics that control catchment export patterns (Moatar and Meybeck, 2005; Godsey et al., 2009; Basu et al., 2010; Musolff et al., 2015, 2017; Zhang, 2018; Minaudo et al., 2019). These studies have proposed that log-transformed relationships between stream discharge and solute or particulate concentrations can be described as chemostatic (stable concentration across all discharge values), or chemodynamic—with either a positive relationship (concentration increases linearly with the log of discharge) or a negative relationship (concentration decreases linearly with the log of discharge). As a log-linear C-Q relationship often does not adequately capture the variability of the data, Meybeck and Moatar (2012) and Moatar et al. (2017) have proposed splitting C-Q curves at the median flow to separately analyze the C-Q relationships during low and high flows.

Our objective is to relate the flow duration curve and C-Q relationship to estimate load flashiness—an indicator of load variability and catchment export (M_2, percentage of cumulative load that occurs during the highest 2% of daily load values). We aim at combining a discharge-based metric (W_2, the percentage of cumulative discharge that occurs during the highest 2% of daily discharge values) with a metric extracted from C-Q analyses (b_{50high}, the slope of the C-Q relationship during high flows) to estimate the M_2 of sediment, sediment-bound particulates or solutes. Furthermore, we examine how this M_2 metric can be used to optimize the sampling frequency for reducing load uncertainty for a large range of catchment types. In order to achieve our objective, we quantify the relationship between W_2, b_{50high}, and M_2 using long-term water quality and discharge datasets of 580 catchments of France and USA in highly diverse geologic, climatic and anthropogenic contexts. Then, we evaluate to what extent this relationship could characterize hydrological and biogeochemical export regimes for dissolved solutes and sediment-bound particulates across contrasting catchments. Finally, we determine the relevance of land cover and geological spatial attributes as predictors for M_2 in drainage basins where no hydrological and or water quality monitoring exist.

DATA AND STUDY SITES

Discharge (Q) and water quality data were obtained from stream databases in 580 catchments in France and the USA (**Table 1**, **Figure 1**). In France (**Table 1A**, **Figure 1A**), we selected monitoring stations that had more than 20 years of daily discharge monitoring and more than 20 years of monthly water quality monitoring of total suspended sediments (TSS), total dissolved solutes (TDS), total phosphorus (TP), nitrate-N (NO_3-N), and dissolved organic carbon (DOC). French daily Q data were extracted from the French river flow monitoring network (HYDRO database, http://www.hydro.eaufrance.fr/). French water quality data (with a median of

---

Abbreviations: W_2, percentage of cumulative discharge that occurs during the highest 2% of daily discharge values, termed as flow flashiness; M_2, percentage of cumulative load that occurs during the highest 2% of daily load values, termed as load flashiness; b_{50high}, slope of the logC-logQ relationship for discharge higher than daily median discharge Q_{50}, termed export pattern; C-Q, concentration-discharge; Q, discharge; Cdf, cumulative distribution function.

TABLE 1 | Summary of datasets.

(A) FRENCH DATA

Parameter	n-Stations		A (km²)	n-Q	q (L s⁻¹ km⁻²)	n-C	C (mg L⁻¹)	Y[a] (kg y⁻¹ ha⁻¹)	Fq50 (%)
Total suspended solids (TSS)	474	Min	13	3,876	1.5	77	2.9	1.7	65.1
		Median	2,915	14,820	12.7	275	19.2	114.9	94.4
		Max	109,966	54,789	59.3	710	182.8	2,358.3	99.7
Total dissolved solutes (TDS)	474	Min	13	3,876	1.5	81	36.3		43.4
		Median	2,915	14,820	12.7	288	401.7		82.0
		Max	109,966	54,789	59.3	748	3,341.2		97.3
Total phosphorus (TP)	475	Min	13	3,876	1.5	59	0.0	0.0	56.6
		Median	2,915	14,820	12.7	241	0.2	0.4	85.2
		Max	109,966	54,789	59.3	613	1.9	3.3	97.9
Nitrate-N (NO₃-N)	475	Min	13	3,876	1.5	80	0.3	0.5	55.5
		Median	2,915	14,820	12.7	281	3.4	11.9	86.6
		Max	109,966	54,789	59.3	1,055	12.3	68.2	99.7
Dissolved organic carbon (DOC)	448	Min	13	3,876	1.5	27	0.9	0.5	57.9
		Median	2,915	14,820	12.7	184	4.1	15.2	87.1
		Max	109,966	54,789	59.3	559	21.5	62.2	98.8

(B) USA, USGS DATA

Parameter	n-Stations		A (km²)	n-Q	q (L s⁻¹ km⁻²)	n-C	C (mg L⁻¹)	Y[b] (kg y⁻¹ ha⁻¹)	Fq50 (%)
TSS	54	Min	660	1,096	0.2	1,096	28.9	45.9	79.2
		Median	7,723	4,383	11.1	4,383	207.4	606.2	97.0
		max	251,149	15,341	46.0	15,341	92,137.7	26,697.3	100.0
TDS	33	Min	743	1,460	0.0	1,460	32.1	No calculations	61.4
		Median	13,177	2,920	3.7	2,920	643.2		74.7
		Max	1,061,441	9,855	52.3	9,855	3,866.9		90.4

(C) USA, ERIE REGION DATA FOR VALIDATION

Parameter	n-Stations		A (km²)	n-Q	q (L s⁻¹ km⁻²)	n-C	C (mg L⁻¹)	Y(kg y⁻¹ ha⁻¹)	Fq50 (%)
TSS	18	Min	11	1,096	9.0	1,096	21.52	145.00	70.1
		Median	1,085	6,940	19.4	6,940	43.48	596.73	89.1
		Max	19,218	16,071	40.2	16,071	108.59	1084.00	98
TDS	16	Min	11	1,096	9.0	1,096	515.90	No calculations	65
		Median	1,085	6,940	19.4	6,940	688.32		78
		Max	19,218	16,071	40.2	16,071	1565.45		89
TP	18	Min	11	1,096	9.0	1,096	0.08	0.20	85.5
		Median	1,085	6,940	19.4	6,940	0.18	0.86	89.4
		max	19,218	16,071	40.2	16,071	0.36	5.76	97.6
NO₃-N	18	Min	11	1,096	9.0	1,096	0.45	1.17	67.3
		Median	1,085	6,940	19.4	6940	2.95	2.83	88.5
		Max	19,218	16,071	40.2	16,071	8.22	52.16	97.5

(A) French dataset (monthly data); *(B)* USA dataset (daily data); *(C)* Erie (USA) dataset (daily data) used for validation. Each table includes the number of stations per parameter (n-Stations), catchment area (A), number of daily discharge data per station (n-Q), mean specific discharge (q), number of parameter concentration data (n-C) per station, mean parameter concentration (C), mean annual load (Y), and solute or sediment total flux that occurs during the highest 50% of daily discharge values (Fq50).

[a] For French sites with monthly concentration data, annual loads calculations are made by reconstructing daily loads with C-Q segmented regression SRC50 described in Raymond et al. (2013).

[b] For US data with daily concentrations, annual loads are calculated as the sum of daily observed loads.

200–300 measurements per station, with up to 1,000 sampling dates for nitrate in some stations) were accessed from http://www.naiades.eaufrance.fr/. The French catchments—from 13 to over 100,000 km² in area—encompassed a wide range of climatic ecoregions (i.e., oceanic, temperate, continental) and geologic, topographic, and hydrologic conditions. From here on, this dataset will be referred as the French database.

We selected sites in the USA (**Table 1B**) that had at least 4 years of daily Q data; some sites had as much as 50 years of such data. We also gathered 4–50 years of data at sites with daily TSS and TDS data. These USA data were accessed via the USGS database (https://waterdata.usgs.gov/usa/nwis/). The selected USA catchments were in temperate or semi-arid ecoregions ranging from 650 to 250,000
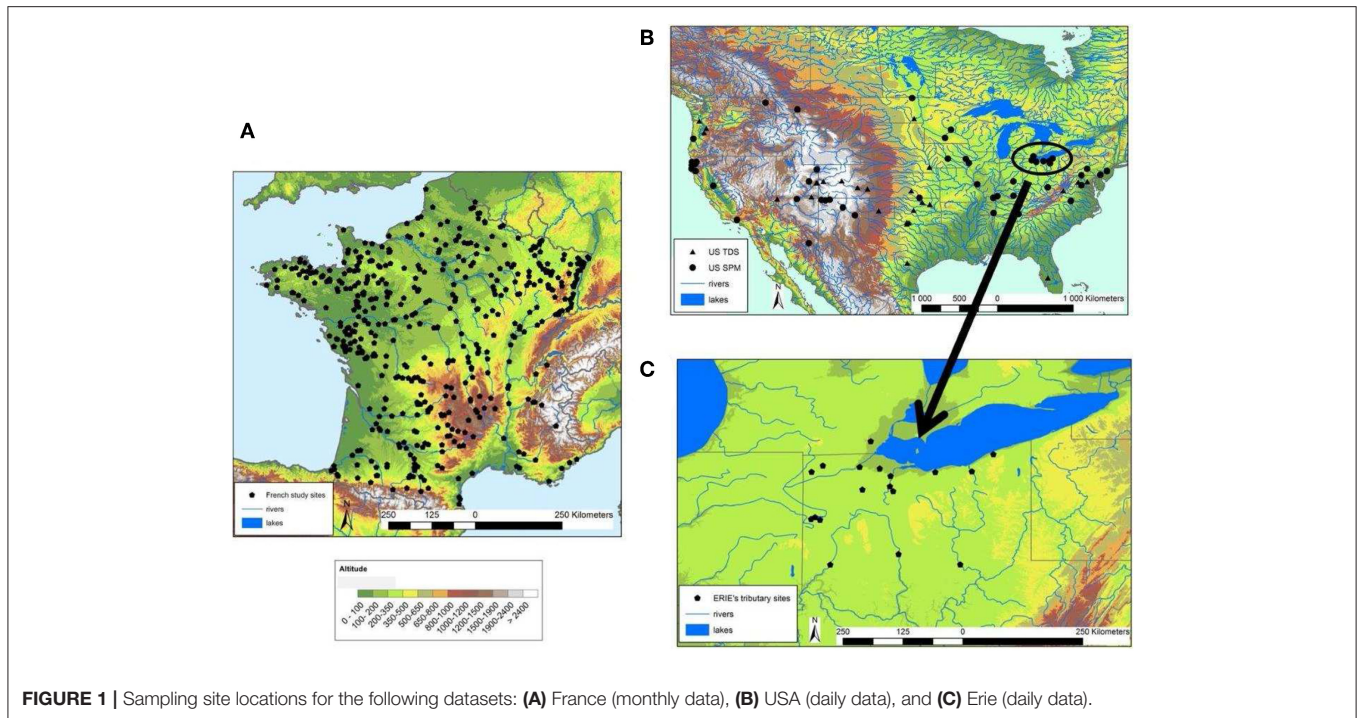
FIGURE 1 | Sampling site locations for the following datasets: **(A)** France (monthly data), **(B)** USA (daily data), and **(C)** Erie (daily data).

km^2. This dataset will from now on be referred as the USA database.

We also selected other USA data to serve as validation sites. The validation dataset encompassed 18 tributaries of Lake Erie (**Table 1C**) monitored by the National Center for Water Quality Research (NCWQR) at Heidelberg University in Ohio, USA. USGS provides the continuous Q data for these monitoring stations. Daily data on TSS, TDS, TP, and NO_3-N, was collected for 4–50 years. Data was accessed at https://ncwqr. org/monitoring. These Erie catchments were under temperate or continental climatic conditions and range in area from 19 to 19,000 km^2. This dataset will from now on be referred as Erie database.

METHODS
Flow and Load Flashiness Indices
Definitions
Flow flashiness can be measured by the proportion of flow being discharged during the $p\%$ highest-flow days. This proportion is often much higher than $p\%$, reflecting the fact that much of the flow is concentrated in a small proportion of time. It theoretically ranges between $p\%$, for a river with constant discharge, to 100% when all the flow is passed in $p\%$ of time.

Formally, let $F(x)$ denote the cumulative distribution function (cdf) of daily discharge. The flow flashiness index Wp is defined as follows:

$$Wp = \frac{\int_0^{p\%} F^{-1}(1-t)\,dt}{\int_0^1 F^{-1}(1-t)\,dt} \tag{1}$$

$F^{-1}(1-t)$ is the flow duration curve (i.e., the daily discharge exceeded with probability t). Wp can therefore be interpreted as the area below the flow duration curve up to $p\%$, relative to the total area below the curve (**Figure 2A**).

In practice Wp can be estimated from an observed series of daily discharge $Q_1, \ldots, Q_n$. Let $Q_{(1)} \geq \ldots \geq Q_{(n)}$ denote the daily discharge sorted in decreasing order, and let $k = \lfloor n*p\% \rfloor$ denote the index corresponding to $p\%$ of the n days ($\lfloor \cdot \rfloor$ is the integer part). Then:

$$Wp = \frac{\sum_{i=1}^{\lfloor n*p\% \rfloor} Q_{(i)}}{\sum_{i=1}^{n} Q_{(i)}} \tag{2}$$

Note that the flashiness index is not restricted to flow variables.

The *load flashiness index* Mp can be computed in the same way as Wp by simply replacing daily discharge (Q) with daily loads (L), calculated as below:

$$L_i = C_i Q_i \tag{3}$$

$$Mp = \frac{\sum_{i=1}^{\lfloor n*p\% \rfloor} L_{(i)}}{\sum_{i=1}^{n} L_{(i)}} \tag{4}$$

Equation (4) allows the calculation of Mp only when daily loads are available. Below, we estimate Mp when daily concentrations and loads are not available.

Differences between Mp and Wp are linked to the properties of the concentration-discharge (C-Q) relationship (Moatar et al., 2013). For perennial rivers, it is possible to mathematically demonstrate the expression of Mp as a function of Wp under the following assumptions (see **Appendix** for the complete details):
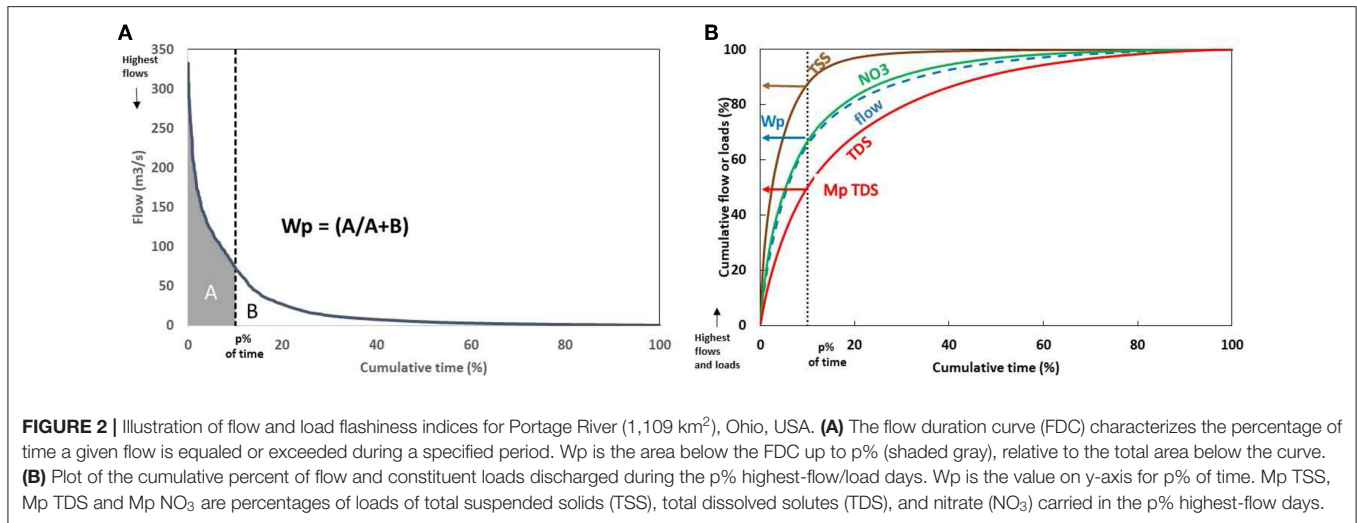
FIGURE 2 | Illustration of flow and load flashiness indices for Portage River (1,109 km^2), Ohio, USA. **(A)** The flow duration curve (FDC) characterizes the percentage of time a given flow is equaled or exceeded during a specified period. Wp is the area below the FDC up to p% (shaded gray), relative to the total area below the curve. **(B)** Plot of the cumulative percent of flow and constituent loads discharged during the p% highest-flow/load days. Wp is the value on y-axis for p% of time. Mp TSS, Mp TDS and Mp NO$_3$ are percentages of loads of total suspended solids (TSS), total dissolved solutes (TDS), and nitrate (NO$_3$) carried in the p% highest-flow days.

i) Daily flows follow a lognormal distribution, i.e., $\log(Q) \sim N(\mu, \sigma)$

ii) Daily concentration can be derived from daily flow using the C-Q regression:

$$\log(C) = a + b.\log(Q) + \varepsilon; \; \varepsilon \sim N(0, \eta^2). \quad (5)$$

The **load flashiness for site i and constituent j**, $Mp_{i,j}$, can be written, under these assumptions, as a function of Wp_i (**flow flashiness for site i**) and the parameters $b_{i,j}$ and $\eta_{i,j}$ of the C-Q regression:

$$\phi^{-1}(Mp_{i,j}) = \phi^{-1}(Wp_i) + \sigma_i \left(\sqrt{(b_{i,j}+1)^2 + \left(\frac{\eta_{i,j}}{\sigma_i}\right)^2} - 1 \right) \quad (6)$$

Where ϕ is the standard normal cdf and ϕ^{-1} its inverse (also known as the probit transformation):

Note that a "good" C-Q relationship would be characterized by a small residual standard deviation ($\eta_{i,j}$) compared with the standard deviation of input log-discharge (σ_i). In such a case, $\frac{\eta_{i,j}}{\sigma_i} \approx 0$ and the relation simplifies to:

$$\phi^{-1}(Mp_{i,j}) = \phi^{-1}(Wp_i) + \sigma_i b_{i,j} \quad (7)$$

Moatar and Meybeck (2007) and Moatar et al. (2013) tested different durations for p% of time (1, 2, 5, 10, 50%) over 125 stations in the USA and several constituents. They distinguished duration curves evaluated for each year and for the whole period of record. The proportion of the highest constituent loads (M_1, M_2... M_{50}) and water volume (W_1, W_2, ... W_{50}) reached in 1, 2 ... 50% of time are key indicators of river-borne material and flows patterns at a given station. They showed that for river TSS, the proportion of fluxes transported during a given percentage of time was always much higher than the proportion of river flow, and conversely, for TDS, this proportion was lower, as shown in **Figure 2B**. They chose the M_2 indicator based on the analysis of statistical distribution of W_1, W_2, ... W_{50}, and M_1,

M_2, ... M_{50} for all water quality variables and stations. M_2 was more accurately defined than M_1. At durations of $p > 5\%$ in certain watersheds (e.g., smaller catchments and/or ephemeral streams with highly flashy and episodic load and flow regimes) the proportion of total annual loading of river-borne material was found to exceed 99%. Given our interest in creating a metric that could be applied across a range of river types and constituents, we set the flashiness index at $p\% = 2\%$ (i.e., M_2 and W_2).

Empirical Approach for Estimating Load-Flashiness (M_2) Depending on Flow-Flashiness (W_2) and Export Pattern (b_{50high})

The formulation proposed in Equation (7) is similar to that proposed by Moatar et al. (2013) based on empirical adjustment, except that here we used a probit transformation for W_2 and M_2. However, our results showed that in many stations, especially for flashy rivers, daily discharge did not follow a lognormal distribution. The Equation (A1) (**Appendix**) for perennial rivers was tested for the French database. W_2 estimated using this equation explained only 46% of the variance of observed W_2 (calculated with Equation 2). Moreover, the dispersion of residuals increased with W_2, i.e., for flashy rivers. Moreover, since log-linear analysis of the full extent of the C-Q relationship often did not adequately capture the variability of the data, Meybeck and Moatar (2012) and Moatar et al. (2017) proposed splitting C-Q curves at the median flow to separately analyze the C-Q relationships during low and high flows. They also demonstrated that, in all cases, the discharge above the median Q value transport between 70 and more than 99% of total load of dissolved and suspended matter. Thus, the exponent b_{50high} (Equation 8) is a relevant control metric of dissolved and particulate material exports.

$$\log C_{Q>Q_{50}} = b_{50high} \log Q_{Q>Q_{50}} + a_{50high} \quad (8)$$

We name this b_{50high} indicator as the "export pattern." Negative b_{50high} values reveal that the cdf of load increases less rapidly than that of river discharge (**Figure 2B**, see TDS curve for

example) defining a dilution processes, either natural (e.g., salt springs) or anthropogenic (e.g., point-source pollution). Positive b_{50high} values express an enrichment or mobilization process (e.g., TSS and TP). Therefore, we replaced "b" in the Equation (7) by "b_{50high}."

Equation (7), demonstrated mathematically, for $p = 2\%$ of time was tested for perennial rivers in the French database and five constituents replacing exponent "b" by "b_{50high}." We compared M_2 estimates obtained with Equation (7) with reconstructed M_2 (see below), for individual constituent and including the whole constituents together. We obtained very good estimates for solutes ($R^2 = 0.96$) and TP ($R^2 = 0.90$), but less for TSS ($R^2 = 0.67$). When we account all constituents, $R^2 = 0.88$.

Since our stations also include intermittent rivers, we decided to use an equation similar to Equation (7), calibrating the parameter α for all stations and constituents (French database and USA database) together (Equation 9). We tested the model by comparing the M_2 predictions with observed M_2 based on a set of independent daily loads for TSS, TDS, TP, and NO_3 (Erie database).

$$\phi^{-1}\left(M_{2i,j}\right) = \phi^{-1}\left(W_{2i}\right) + \alpha \, b_{50high_{i,j}} \qquad (9)$$

for site i and constituent j, the calibrated α coefficient is 0.79.

This equation (Equation 9) explained 91% of M_2 variance based on the French reconstructed daily loads using the C-Q relationship and the USA daily database with a root mean square error (RMSE) of 4% (**Figure S1A**). Moreover, for the Erie database (**Figure S1B**; not included in the calibration), 91% of variance of M_2 is explained with W_2 and b_{50high}; the RMSE is 5%. Therefore, the combination of b_{50high} and W_2 constitutes a good proxy for M_2 estimation when daily concentration data are not available.

M₂ Reconstruction and Robustness From Discrete Concentrations Surveys and Daily Discharge

Reconstructed M2

To calibrate the parameter α on Equation (9), we used "true M_2," calculated from daily load available for USA database with Equation (4) and "reconstructed M_2" calculated from monthly French database. Reconstructed M_2 were determined after reconstruction of daily concentrations based on daily discharge using a segmented linear regression (Method SRC₅₀ tested by Raymond et al., 2013) and Equations (8) and (10).

$$logC_{Q<Q_{50}} = b_{50low} \log Q_{Q<Q_{50}} + a_{50low} \qquad (10)$$

Q_{50} is the median discharge estimated from daily discharge. We tested statistical significance of C-Q correlation by Pearson product-moment correlation, with significant relationships ($p < 0.05$) depending on the slope. Most slopes were significant when $b > 0.2$ (Meybeck and Moatar, 2012), although the actual threshold varied depending on the number and variance of C-Q couples in the regression. We reported in **Table S2**, percentages of sites with significant correlations ($p < 0.05$) for segmented C-Q regressions.

To assess the robustness of M_2 estimates derived from discrete surveys, we used two methods.

i)   We validated the predictions of Equation (9) (M_2 predicted) using the Erie database with "true M_2" for four parameters and 18 rivers.

ii) We compared M_2 estimates, obtained after the reconstruction of daily concentrations by segmented linear regression approach (Equations 8 and 10) with those obtained using the Weighted Regression on Time, Discharge, and Season approach (WRTDS; Q. Zhang pers. Comm.; Hirsch et al., 2010), a commonly used method (Lee et al., 2016; Zhang, 2018; Zhang et al., 2019). This was done on 248 French stations where monthly data of TSS, TP, and NO_3, and daily Q where available for more than 40 years.

Analysis of b₅₀high and M₂ Variability Across Decades and Years

Equation (9) has been used with M_2, W_2, and b_{50high} calculated from the entire set of data (between 20 and 40 years long). Since C-Q relationships can change with time, for example due to land use change, we assessed the stability of b_{50high} and M_2 across decades. To do so, we used the French dataset in four successive series of 10 years, i.e., 1978–1987; 1988–1997; 1998–2007; 2008–2017. Tukey's range test was used for the comparison of M_2, b_{50high}, and W_2 across four decades and for the whole 40-y period to find means that are significantly different from each other. Additionally, we analyzed annual b_{50high} variation for five stations in the Erie dataset where more than 35 years were available.

Minimal Length of Monitoring Required

We investigated the sensitivity of period length on estimated b_{50high} and M_2 considering monthly sampling (12 C-Q pairs per year). We used as reference the metrics computed from daily TSS, TDS, TP, and NO_3, surveyed for more than 30 years in four rivers from the Lake Erie dataset with various watershed scales (386–15,395 km^2). To mimic a classic long-term monthly monitoring, daily concentration time series were randomly subsampled following a normal distribution (30 days average ± 5 days). The metrics b_{50high} and M_2 were then computed on subsampled data and compared to reference values. To assess potential variations due to varying sampling dates, this was repeated 100 times for each given period length. We investigated this from 2 years-long timeseries, up to 20 years.

Determination of the Optimal Sampling Frequency

We used the formulations proposed by Moatar et al. (2013) to predict the magnitude of uncertainties (bias and precision) of loads and mean concentration using the discharge-weighted method. This method is commonly used by the Helsinki Commission (HELCOM) Baltic Sea Action Plan and by the Convention for the Protection of the Marine Environment of the North-East Atlantic (OSPAR), international European
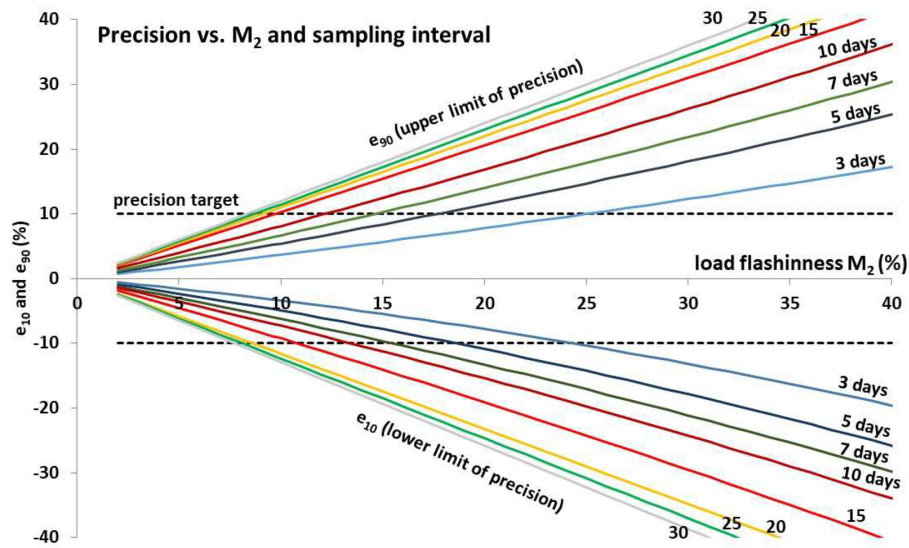
FIGURE 3 | Error nomograph (e_{10}, e_{90} vs. M_2) for annual loads calculated for discharge-weighted concentration method (adapted from Moatar et al., 2013). Lower limits (e10) and upper limits (e90) for sampling intervals of 3, 7,..., 60 days. M_2 is the percentage of cumulative load that occurs during the highest 2% of daily load values.

conventions on river pollutant loads to coastal zone (Littlewood and Marsh, 2005). The equations are:

$$e_{10} = r(d)^* M_2^2 + s(d)M_2 \qquad (11)$$

$$e_{90} = u(d)^* M_2^2 + v(d)M_2 \qquad (12)$$

where e_{10} and e_{90} = lower and upper limits of precision; d = sampling interval in days; r, s, u, v values for calculating precision for different d are available in **Table S1**. We used this formulation to derive an optimal sampling monitoring given an imposed $\pm 10\%$ as a level of precision (**Figure 3**). See Moatar et al. (2013) for more explanation on the method and formulations for biases.

Relationship Between Catchment Characteristics and W_2, b_{50high}, and M_2

We analyzed the main geographical, geological and land cover characteristics of 475 French drainage basins. We then determined relationships between these variables and W_2, b_{50high}, and M_2 for each of the water quality parameters. We performed generalized additive model (GAM) to assess potential non-linearity in relationships. The results showed that smoothing functions poorly improved the regression models. Hence, we assumed that classical multivariate regressions would be convenient to highlight and discuss simple relationships including their sign.

We used multiple linear regressions to evaluate the relationship between French dataset characteristics, i.e., catchment size, agricultural land use, lithology, wetland surface, stream network density, erosion indicator risk, as well as W_2, b_{50high}, and M_2 for each of the water quality parameters, i.e., TSS, TDS, TP, NO_3, and DOC. These variables are listed with full details provided in **Table 2**. Starting with all explanatory variables in initial regression models, we used a backward

selection approach to select only the significant ones (at $p < 0.001$). To assess the relative contribution of the selected variables, a hierarchical variation portioning was performed on each final model using the R package hier.part (Walsh and MacNally, 2013).

RESULTS

Flow-Flashiness (W_2) and Export Pattern (b_{50high}) Indicators

The interannual flow-flashiness indicator of the study sites (W_2) ranged between 3 and 60%, with the majority between 5 and 30% (**Figure 4**). The high W_2 values were obtained for USA semi-arid sites (W_2 = 48% for San Pedro River, Arizona; 60% for Santa Clara River, California) and the French Mediterranean catchments (W_2 = 39% for Agly River, Pyrénées Orientales). Low W_2 values were found for groundwater-influenced streams (W_2 = 3% for Ill River, France), glacial or nival regimes (W_2 = 7% for Arve River and Romanche River, Alps, France), or by impoundments (W_2 = 4% for Columbia River near Quincy, OR, USA or 6% for the Rhône River in France).

The range of b_{50high} varied depending on the water quality variables considered; but for a given variable, the range obtained from monthly sampling data (French dataset) did not significantly differ from the ones obtained from daily sampled data (USA dataset; **Figures 4A,B**). More specifically, TSS generally presented a positive chemodynamic pattern with b_{50high} values $> +0.2$ and reaching up to 3 (**Figure 4A**). For the French dataset, high positive b_{50high} values generally corresponded to streams with low flashiness, i.e., $W_2 <$ 15%. Some catchments in the Alps' mountains with snow hydrological regime (low W_2) and influenced by hydroelectric

TABLE 2 | List of explanatory variables and their definitions, units, and data sources.

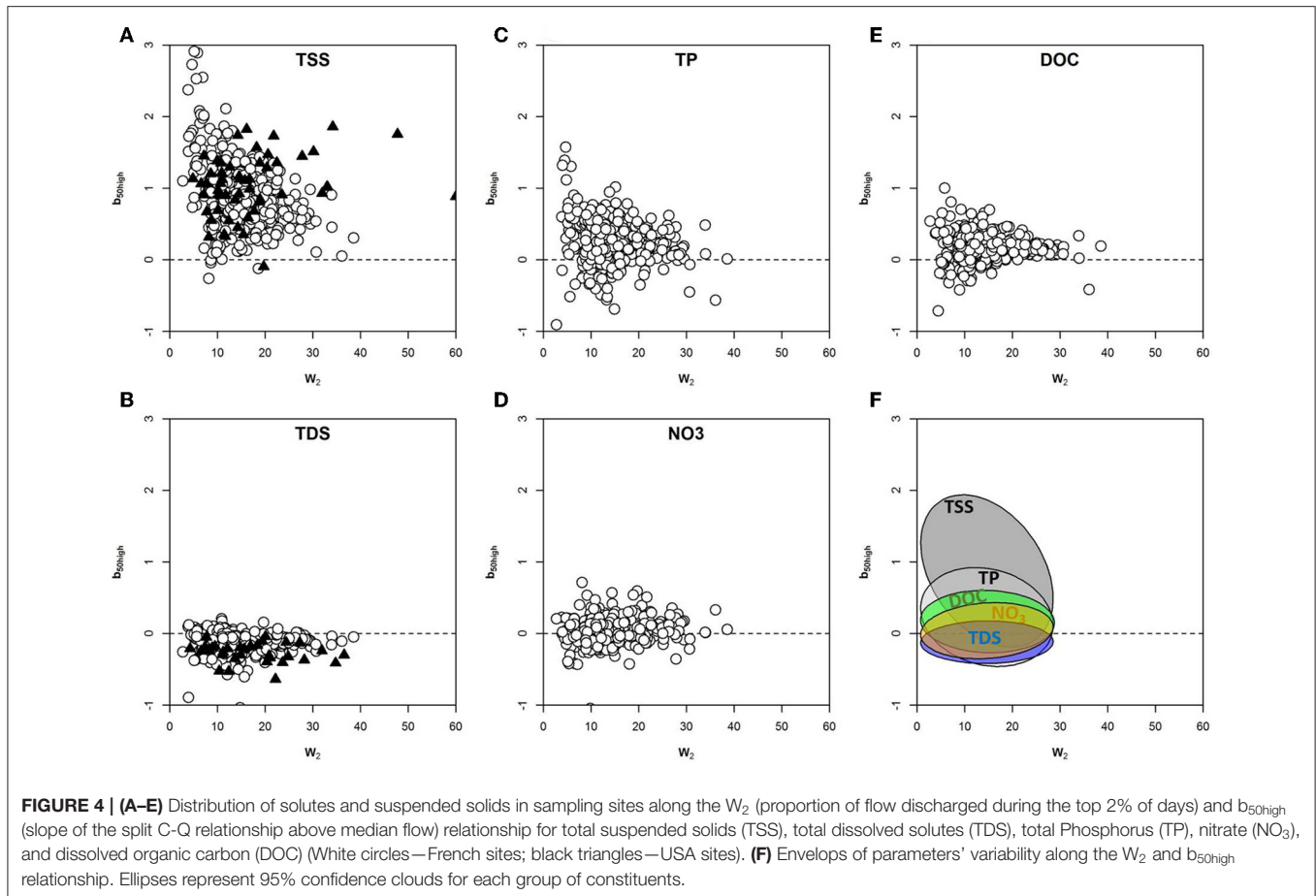| Variable	Definition	Unit	Source
Area	Drainage area of the water quality monitoring station	km^2	
Stream network density	Density of the natural stream network in the catchment	km/km^2	BDCarthage v4 IGN
Wetlands	Percentage of potential wetland in the catchment	%	INRA – Beven index (Quinn et al., 1995)
Crystalline rocks	Percentage of crystalline rocks in the catchment	%	BRGM 1/1,000,000
Low carbonate rocks	Percentage of low carbonate rocks in the catchment	%	BRGM 1/1,000,000
High carbonate rocks	Percentage of high carbonate rocks in the catchment	%	BRGM 1/1,000,000
Riparian vegetation	Percentage of riparian vegetation in a 10 m wide buffer on both sides of the stream	%	SYRAH_CE
Forest	Percentage of forest in the catchment	%	CORINE Land Cover EEA 2012
Extensive agriculture	Percentage of extensive agriculture in the catchment	%	CORINE Land Cover EEA 2012
Intensive agriculture	Percentage of intensive agriculture in the catchment	%	CORINE Land Cover EEA 2012
Urban area	Percentage of urban land use in the catchment	%	CORINE Land Cover EEA 2012
Population density	Number of inhabitants divided by the catchment area	Inhabitant/km^2	INSEE 2011
Point source P	Sum of domestic and industrial phosphorus point sources loads	kg P/ha/year	AELB[a]
Soil P	Total phosphorus content in the surficial soil horizon.	g/kg	INRA (Delmas et al., 2015)
Point source N	Sum of domestic and industrial nitrogen point sources loads	kg N/ha/year	AELB[a]
N surplus	Balance between nitrogen added to an agricultural system and nitrogen removed from the system per hectare of agricultural land	kg N/kg	NOPOLU 2010 (Schoumans et al., 2009)
Erosion risk	Fraction of area with a strong to very high hazard erosion (derived from land use, topography, and soil properties)	%	INRA (Cerdan et al., 2010)

[a]http://www.eau-loire-bretagne.fr/informations_et_donnees.

dams were characterized by a very high export pattern (b_{50high} between 2 and 3) due to yearly flushing dam management to maintain river-bed sediment dynamics and to prevent siltation (Nemery et al., 2013). Some coastal Californian stations (Eel and Santa Clara Rivers) and Colorado Plateau streams (San Pedro and Paria Rivers) presented both high W_2 and b_{50high} for TSS. On the contrary, TDS generally showed a negative chemodynamic pattern, i.e., dissolved ions are diluted when discharge increases (**Figure 4B**), regardless of the flow flashiness (W_2).

TP, often transported with sediment, followed a similar pattern as TSS but with a smaller range of variation (**Figure 4C**). A positive export pattern (b_{50high}) for TP was found for 84% of data with most export pattern values < 1. The b_{50high} for TP was negative for 16% of data indicating dilution. Seventy percent of NO_3-N presented a chemostatic pattern across all values of flow flashiness considered (**Figure 4D**). Nitrate mobilization in the drainage basins was proportional to discharge. DOC also presented a positive chemodynamic pattern for 50% of the studied catchments, but the high W_2 sites were characterized by a more stable, chemostatic pattern (**Figure 4E**). Envelops of variability of the b_{50high}-W_2 relationship presented a rather distinctive shape, even though parameters overlapped (**Figure 4F**, ellipses represent 95% confidence clouds for each group of constituents).

The variability of annual W_2 differed depending on climate and catchment hydrology. Differences between maximal and minimal annual W_2 values ranged between 40 and 60% for catchments exposed to a contrasting climate (e.g., small catchments in the Mediterranean area experiencing hot and dry summers and intense short rainy events in autumn; catchments with no storage capacity resulting in severe low-flow and quick runoff response to rainfall events). Ranges <20% were observed for streams fed by large aquifers (e.g., northern France) or in catchments where snow pack storage buffers the variability of daily flows.

Variability of Load Flashiness (M_2)

Interannual load-flashiness indicator values ranged between 2% (TDS for Ill River at Strasbourg) and 98% (TSS at Santa Clara River)—close to the possible range (2–100%) (**Figure 5A**). The distribution of M_2 values was highly skewed, with 50% of values lower than 22%, and 75% lower than 27%. The range of M_2 varied between solutes; M_2 increased in the following order: TDS, NO_3, DOC, TP, and TSS. Based on this statistical distribution of M_2, we defined five classes. The upper boundary of the lowest class was 8% with each subsequent boundary representing a doubling of the prior upper limit. The median class contained the median statistical distribution value. The very low class of flashiness (M_2 ranging between 2 and 8%) corresponded to

FIGURE 4 | (A–E) Distribution of solutes and suspended solids in sampling sites along the W_2 (proportion of flow discharged during the top 2% of days) and b_{50high} (slope of the split C-Q relationship above median flow) relationship for total suspended solids (TSS), total dissolved solutes (TDS), total Phosphorus (TP), nitrate (NO_3), and dissolved organic carbon (DOC) (White circles—French sites; black triangles—USA sites). **(F)** Envelops of parameters' variability along the W_2 and b_{50high} relationship. Ellipses represent 95% confidence clouds for each group of constituents.

negative or low b_{50high} and low W_2 (**Table 3**, **Figures 5A,B**). The low class of flashiness corresponded to M_2 between 8 and 16%. The medium class of flashiness corresponded to M_2 between 16 and 32%. The high class of flashiness corresponded to M_2 between 32 and 64%. The very high class of flashiness ($M_2 >$ 64%) corresponded to strongly positive b_{50high} and high W_2. The proportion of the total number of studied stations in each class of load flashiness varied according to the constituents (**Table 3**). DOC, NO_3, and TP generally were found in the low and medium load flashiness classes, while TSS was found in medium and high classes. TDS was more widely distributed between very low, low, and medium load flashiness classes. The relationship between M_2 and W_2 were similar on an annual and interannual basis (**Figure 5**). On both annual and interannual basis, M_2 was generally higher than W_2, i.e., points above the 1:1 line, for all the constituents (with positive b_{50high}), except TDS which present mostly negative b_{50high}.

Using Equation (9), we drew M_2 isolines representing the five classes' limits on the W_2–b_{50high} relationship (**Figure 6A**). The diagram permitted comparisons of M_2 values between streams and/or presents the M_2 differences between constituents for a given stream, as illustrated for four tributaries of the Lake Erie, USA with contrasting W_2 (**Figure 6B**). The diagram of solute and export regime is presented in **Figure 6C**.

M_2 and b_{50high} Robustness
Influence of the Concentration Reconstruction Method to Estimate M_2

The two methods used to reconstruct daily concentrations led to similar results. The standard deviation of differences in the estimates of M_2 calculated with daily concentrations reconstructed with the WRTDS and the segmented C-Q method (M_{2WRTDS}-M_{2SRQ50}) was around 4% for NO_3 and TP for the four decades considered and 12% for TSS (Data presented in **Figure S2**). The mean difference of M_2 estimates was zero for NO_3, but it was +4% for TSS and +2% for TP. For these two last parameters, M_2 estimated by WRTDS method were larger than estimates for the C-Q segmented method (**Figure S2**).

Analysis of b_{50high} and M_2 Variability Across Decades and Years

For the French dataset, where we have up to 40 years of data, b_{50high} for TSS, TDS, NO_3, and DOC showed little variation across decades, while we found some noticeable, but not significant differences for TP. Overall, the variability between the four decades was limited for TSS (<5% for median M_2 and <0.05 for median b_{50high}), TDS, DOC and nitrate (<1% for M_2). For TP, b_{50high} was higher in the last period (2008–2017) (+0.2) than in first and second periods (1978–1987 and 1988–1997).
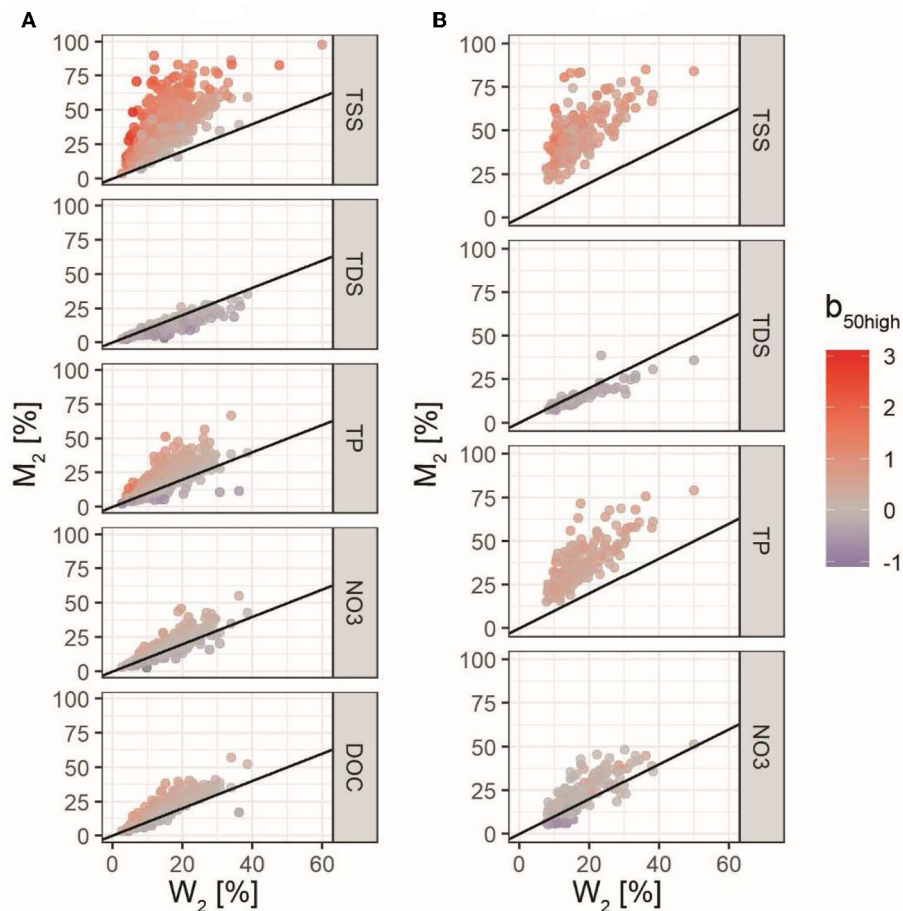
FIGURE 5 | (A) Relationship between interannual M_2 (load flashiness) and W_2 (flow-flashiness) for monthly French dataset and daily USA dataset, computed for total suspended solids (TSS), total dissolved solids (TDS), total phosphorus (TP), nitrate (NO_3), and dissolved organic carbon (DOC). **(B)** Relationship between annual M_2 and W_2 for daily Erie dataset, computed for total suspended solids (TSS), total dissolved solids (TDS), total phosphorus (TP), and nitrate (NO_3). Dot color is a function of b_{50high} (slope of the logC-logQ relationship for discharge higher than daily median discharge Q_{50} values); see color scale inserted in the right of the figure.

This was due to a more pronounced dilution of punctual sources which were more important in the 1978–1997. Therefore, the load-flashiness was lower (−5%) in the first period compared to the present time. However, the differences were limited.

For yearly variations in the Erie dataset, differences were more important across years, which was particularly true for Cuyahoga and mostly for TSS, TDS, and TP (**Figures S3**, **S4**). For the other studied rivers, the variations of annual b_{50high} were more limited, even if some years could have a more pronounced export pattern (b_{50high}).

Minimal Length of Monitoring Required for Determining b_{50high} and M_2

Sensitivity of period length necessary to derive reliable b_{50high} and M_2 estimates from monthly monitoring was assessed via subsampling of daily timeseries (**Figure 7**). Results showed site-specific and metric-specific sensitivities but overall differences between monthly-based (median after 100 random draws) and daily-based values were systematically decreasing with longer period length. Relative bias was smaller for b_{50high} and higher

for M_2, in particular for TSS at Honey Creek station which was the only timeseries presenting large bias (−62% bias even for timeseries longer than 10 years). Variability across the 100 random draws was reduced for both metrics computed from longer timeseries and for all constituents despite larger variability for b_{50high} computed for NO_3 data (±60%). Results indicated that 10 years-long monthly timeseries represented a reasonable amount of observations for coherent estimation of these two key metrics.

Implications for Sampling Frequency

The optimal sampling frequency needed to minimize the uncertainty associated with the estimation of solute and sediment loads increased with increasing M_2 (**Figure 8**). Based on Equations (11) and (12), we obtained that for M_2 of 8% or less, a monthly sampling would be sufficient to obtain load estimation with 10% of precision. If M_2 was 16%, a weekly sampling would be required to keep the same level of precision. If M_2 was more than 32%, a sub daily sampling would be necessary.

The comparison of the optimal frequencies to calculate annual loads with <10% precision using our approach and the current sampling frequency recommended by the European Water Framework Directive is presented in **Figure 9**. This revealed that more than 90% of the existing monitoring strategies would fail to accurately calculate annual loads of solutes and particulates transported by French streams and rivers with the Q-weighted concentration method, a method commonly used by HELCOM and OSPAR international European conventions on river pollutant loads to coastal zone. The load-flashiness diagram informed that each catchment and constituent needs specific monitoring strategies to obtain load estimates with good precision. TDS needs lower sampling frequencies than NO_3 and DOC. Also, constituents associated with suspended sediments, like TP, need more frequent sampling. TSS required high frequency for the majority of stations. The median of

optimal sampling interval between two measurements required for the French dataset was: 13 days for TDS, 8 days for NO_3, 6 days for DOC, 5 days for TP, and every day sampling for TSS.

Influence of Catchment Characteristics on Nutrient, Carbon, and Sediment Export Regimes

Catchment characteristics explained up to 38% of the total variance of W_2, b_{50high}, and M_2 (**Table 4**; first line). Individual contributions (between 0 and 100%) of the selected variables (see **Table 2**) according to hierarchical variation partitioning are indicated below. In **Table 4**, blue and red cells indicate positive and negative relationships, respectively.

W_2 was positively related to the stream network density and the percentage of intensive agriculture in the catchment (25 and 13% respectively) while it decreased with the size of the drainage basin (21%). The b_{50high} values of TSS, TP and DOC (between 31 and 44% of variance explained) decreased with the percentage of crystalline rocks in the catchments. We found a significant positive relationship between the percentage of wetland in the catchment and the DOC b_{50high} (21%), while a negative relationship was found for TSS b_{50high} (19%). The percentage of intensive agriculture in the catchment had a significant positive influence on TDS b_{50high} (18%). Load flashiness (M_2) decreased with the size of the catchment for all the water quality parameters, while it increased also for all the water quality parameters with the stream network density and the percentage of intensive agricultural practices.

DISCUSSION

Load Flashiness (M$_2$) Evaluation With Flow Flashiness (W$_2$) and Export Pattern (b$_{50high}$)

We found that load flashiness (M2) can be inferred from flow flashiness (W2) and export pattern (b50high) based on a large
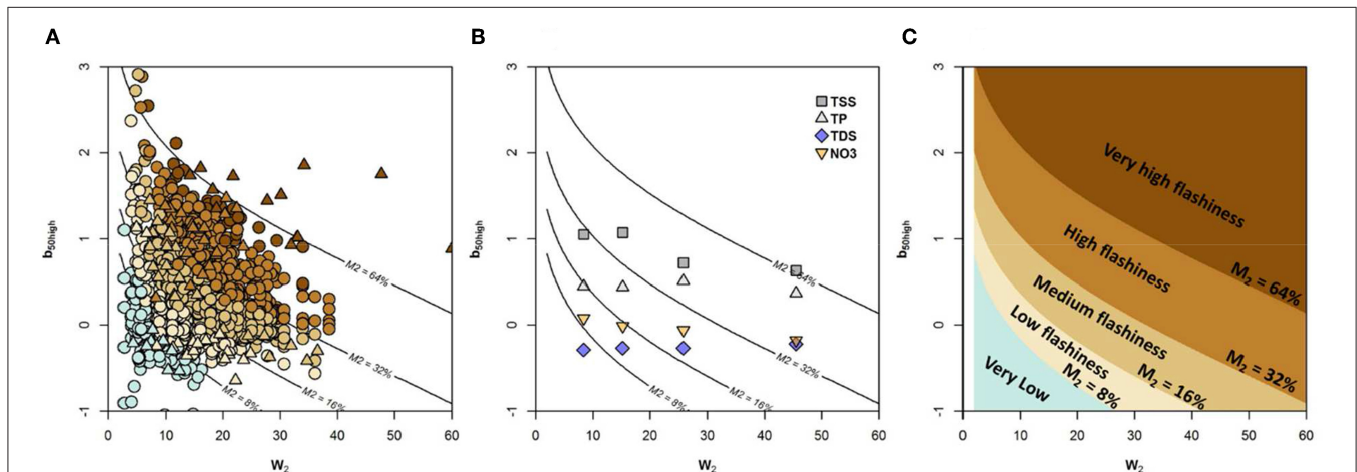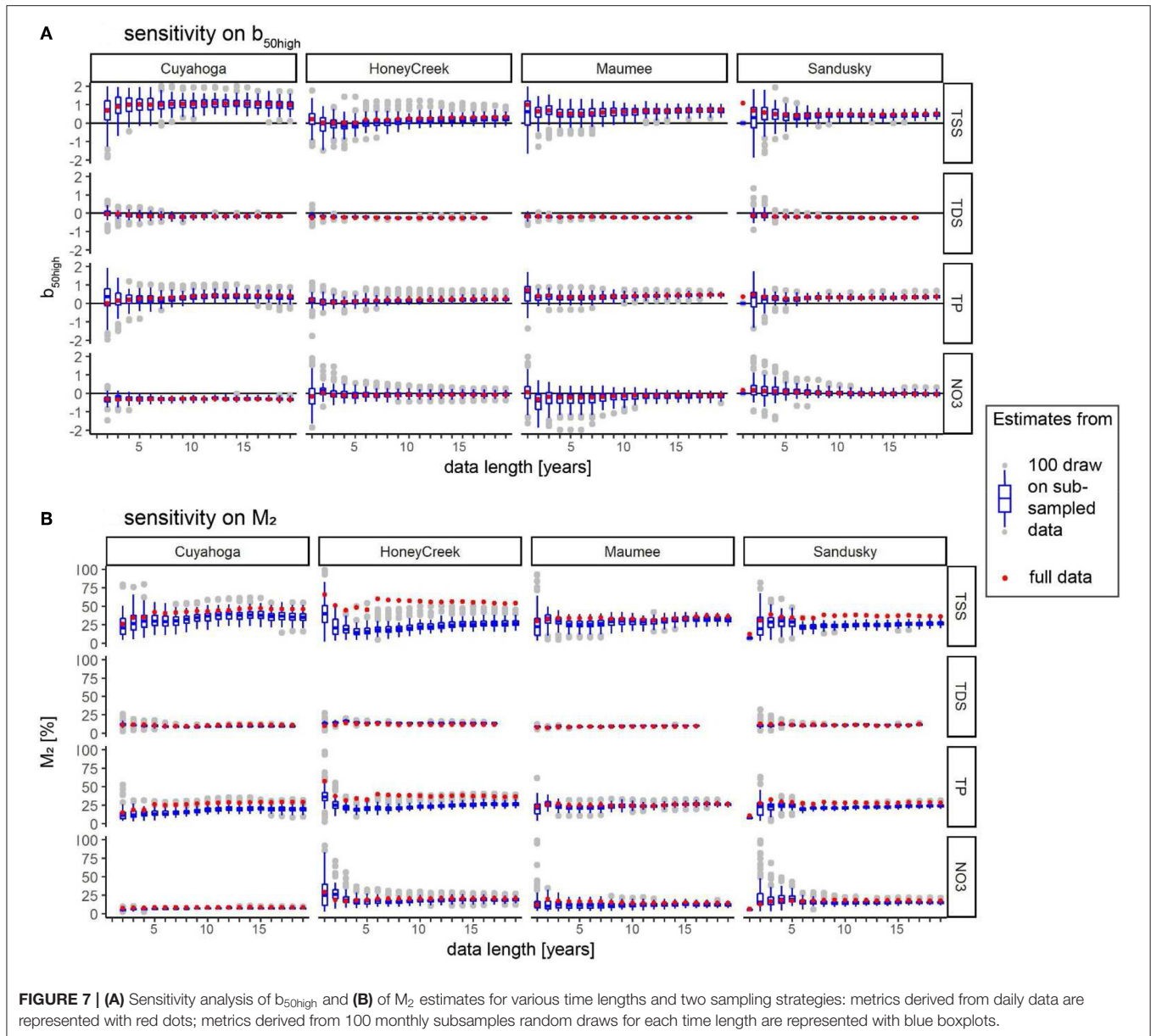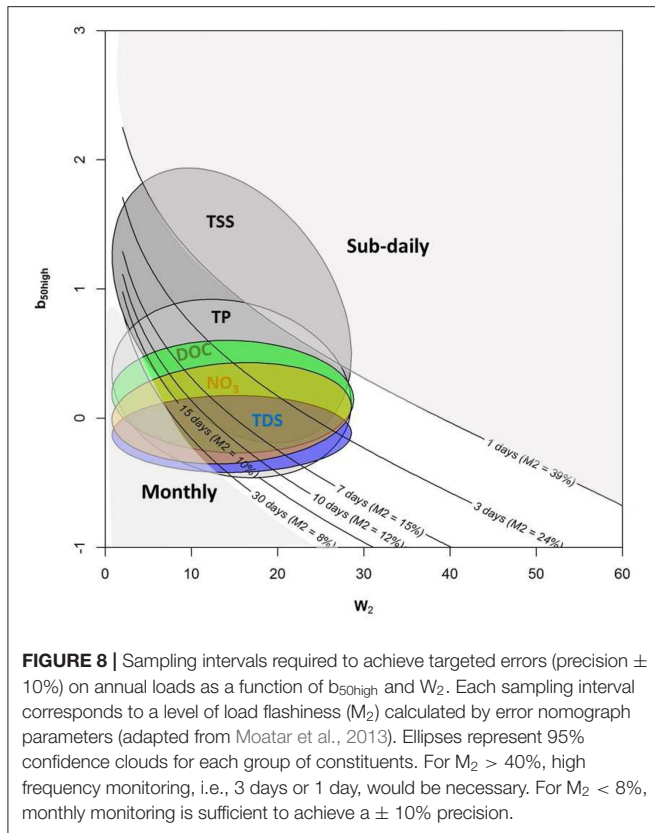
TABLE 3 | Distribution of the 2,507 sample series (percentage) in each class of load flashiness depending on the solutes or particulates.

	Very low	Low	Medium load flashiness	High	Very high
	$M_2 < 8\%$	$8\% < M_2 < 16\%$	$16\% < M_2 < 32\%$	$32\% < M_2 < 64\%$	$M_2 > 64\%$
TSS	0	6	33	52	8
TDS	19	62	20	0	0
TP	7	35	48	10	0
NO_3	8	48	39	4	0
DOC	6	39	49	7	0

TSS, total suspended solids; TDS, total dissolved solutes; TP, total phosphorus; NO_3, nitrate; DOC, dissolved organic carbon.

FIGURE 6 | (A) Representation of the load flashiness M$_2$ indicator (load flashiness) as a function of W$_2$ (flow-flashiness) and b$_{50high}$ (export regime). Each color represents a class of flashiness. The color of the points corresponds to the class given by the observed M$_2$. The lines are derived from Equation (9). **(B)** Examples of M$_2$ values for four water quality parameters (TSS, TDS, TP, and NO$_3$) of four Erie Lake tributaries of increasing areas. The color of the points corresponds to the class given by the observed M$_2$. The lines are derived from Equation (9). **(C)** Diagram of load flashiness and five classes of flashiness from very low flashiness with M$_2 < 8\%$, to very high flashiness with M$_2 > 64\%$.

FIGURE 7 | (A) Sensitivity analysis of b_{50high} and **(B)** of M_2 estimates for various time lengths and two sampling strategies: metrics derived from daily data are represented with red dots; metrics derived from 100 monthly subsamples random draws for each time length are represented with blue boxplots.

dataset of stream concentration and discharge encompassing a wide range of climatic, geologic and land use conditions. We characterized the flashiness of solute and sediment export regime (M_2) using hydrological and biogeochemical indicators calculated for high flows, i.e., the flow flashiness (W_2) and the exponent of C-Q relationships during discharge higher than the median (b_{50high}). Following previous studies, we determined that stream export of solute and sediment during the highest 2% of time (M_2) was a good indicator of solute and sediment transport. We proposed to overcome the lack of high frequency concentration measurements by using the exponent of C-Q relationships during high flow periods (b_{50high}) as a proxy for export pattern, coupled with flow flashiness—a parameter more easily available, thanks to continuous discharge monitoring or

new modeling development for ungauged catchments (Oudin et al., 2008).

The theoretical proposed approach is based on two assumptions which have some implicit limitations. The first assumption (see **Appendix** for detailed demonstration) is that the distribution of daily Q is lognormal with parameters μ (mean of logarithms) and σ (standard deviation of logarithms). However, daily flow might not be lognormal. For instance, in intermittent streams, a specific term may be needed to describe the occurrence of zero flows. Moreover, the distribution of daily flows may be heavy-tailed leading to more extreme flows than suggested by the lognormal distribution. Therefore, flow variability might be described by other metrics in addition to σ, such as the probability of zero flows or

FIGURE 8 | Sampling intervals required to achieve targeted errors (precision $\pm$ 10%) on annual loads as a function of b_{50high} and W_2. Each sampling interval corresponds to a level of load flashiness (M_2) calculated by error nomograph parameters (adapted from Moatar et al., 2013). Ellipses represent 95% confidence clouds for each group of constituents. For $M_2 > 40\%$, high frequency monitoring, i.e., 3 days or 1 day, would be necessary. For $M_2 < 8\%$, monthly monitoring is sufficient to achieve a $\pm$ 10% precision.

some tail coefficient. The second assumption is that the daily concentration C can be derived as a power function of the daily flow, $C = aQ^b$. This implies that the daily load is equal to:

$L = CQ = aQ^{b+1}$ which is a raw approximation. In particular, C-Q data typically show a large scatter around this power relationship. This scatter creates an additional source of variability that might play a non-negligible role on the variability of loads, and hence on the flashiness M_2. The regression formula of Equation (7) could therefore be augmented with an additional predictor describing the variability of the residuals around the C-Q power relationship.

Despite these assumptions, the theoretical model for perennial rivers (Equation 7), and the empirical model (Equation 9) provide good predictions of load flashiness (M_2). The empirical model (Equation 9) was parameterized based on an extensive monthly-sample data set from France (TSS, TDS, TP, NO_3, and DOC) and daily-sample data set from USA (TSS and TDS). The model was validated using an extensive daily-sample dataset (TSS, TDS, TP, and NO_3) from several rivers near Lake Erie. However, a more diverse validation dataset would have been desirable. Yet, daily concentrations with long-term time series are very rare.

M_2 can be calculated by different methods depending on sampling frequency of concentration. When high-frequency concentration data are available, daily loads can be derived and Equation (4) can be applied. When discrete surveys are available, for example monthly samples, there are two
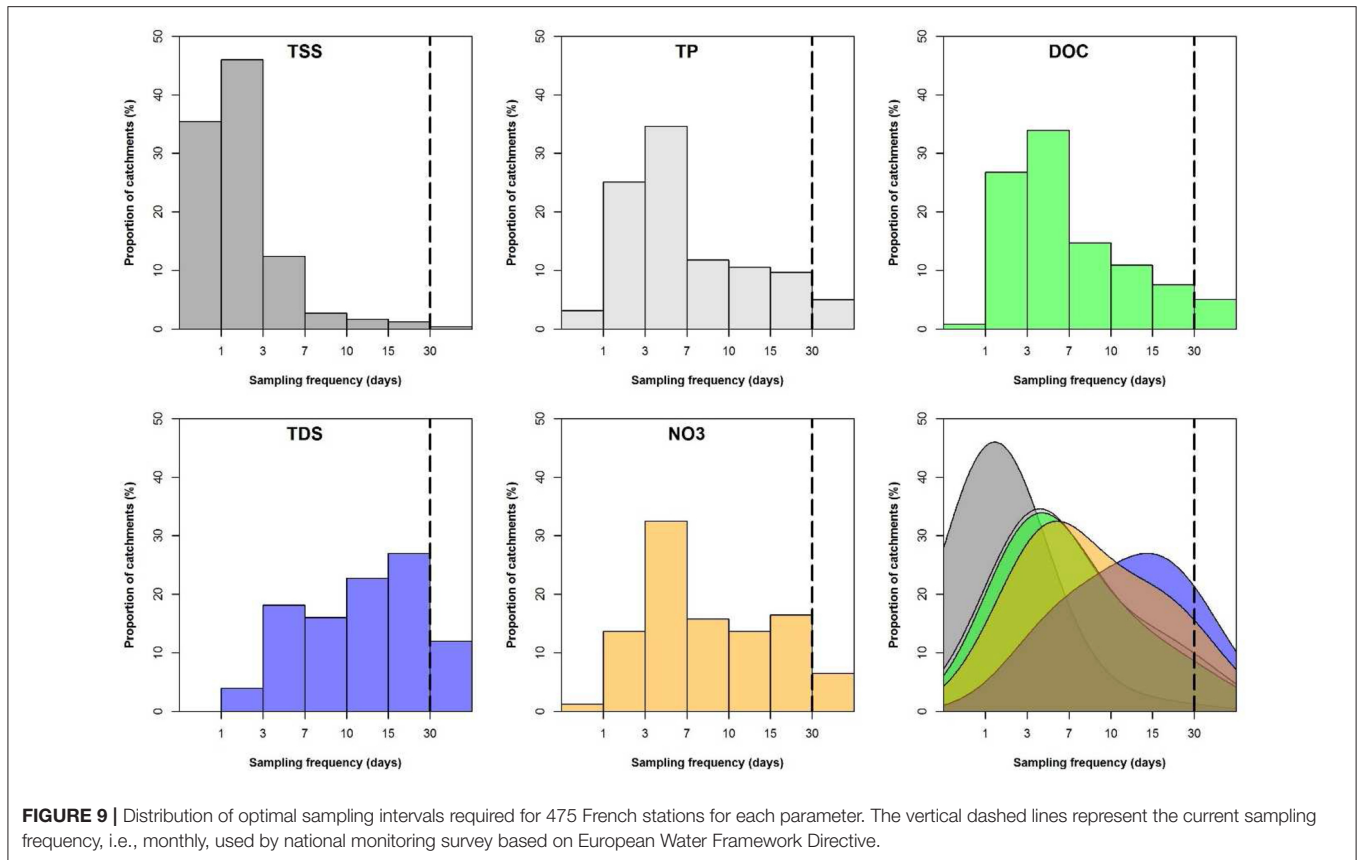
options to characterize the M_2. One can apply Equation (4) after reconstruction of daily concentrations with a regression method like WRTDS (Hirsch et al., 2010) and LogC-LogQ regression (Raymond et al., 2013; Moatar et al., 2017; Minaudo et al., 2019). Or it is possible to apply theoretical (Equation 7) (for perennial rivers) or empirical (Equation 9), both depending on W_2 and export pattern (b_{50high}). W_2 can be easily determined, and b_{50high} can be predicted depending on constituent. For example, the diagram of load-flashiness (**Figure 6C**) can give indicative values of classes of flashiness depending on these two indicators. The choice of 2% duration to define flow and load flashiness was suggested here to be representative of duration for many constituents. If studies focus on specific constituents, the question of choice of duration could be evaluated. For example, Frazar et al. (2019) analyzed durations of 2, 5, and 10% to characterize contrasting behavior of nitrate and phosphate loads from high flow events on small catchments. Moreover, this approach allows the decoupling of flow flashiness and export pattern to discern distinct patterns which could be related to drainage basin characteristics, climate change or land use change (**Table 4**, discussed below).

Characterization of Solute and Sediment Export Regimes Across Various Range of Catchments

Our databases cover a wide range of climatic, lithological, land use and hydrological conditions found in the northern hemisphere between 30° and 50°N and range across river magnitudes from 10 km^2 to 1 million km^2. The database displays extensive ranges of concentration and river flow which are close to those observed at the global scale for river basins of similar sizes (Meybeck and Helmer, 1989; Meybeck et al., 2003). We argue that the ranges of the indicators obtained here are also close to their global distributions in these latitudes, and thus our results can provide guidance in many settings.

C-Q relationships are important signatures of catchment biogeochemical processes and export regime (Moatar et al., 2017). Separately analyzing the C-Q relationships during low and high flows improves estimates of non-linearity and potential shift effects in hydrological and biogeochemical controls under different hydrological regimes (Underwood et al., 2017; Diamond and Cohen, 2018). The range of export pattern, b_{50high}, is more contrasted than b calculated from the whole hydrograph, as conducted by Godsey et al. (2019) in a similar large database.

The relationship between discharge and concentration has significant implications for the inequality of solute export dynamics. Indeed, differences between cumulated percentage of load and flow associated with a specific duration or the ratios of Gini coefficients depend on the C-Q relationship (Jawitz and Mitchell, 2011; Moatar et al., 2013). If the C-Q relationship is chemostatic (b = 0, constant C), discharge and load have the same Gini Coefficients ($G_L/G_Q = 1$). When C-Q relationship is negative (b < 0), often indicating a dilution signal, the inequality of load is smaller than discharge ($G_L/G_Q < 1$). When C-Q relationship are positive (b > 0) revealing an enrichment

FIGURE 9 | Distribution of optimal sampling intervals required for 475 French stations for each parameter. The vertical dashed lines represent the current sampling frequency, i.e., monthly, used by national monitoring survey based on European Water Framework Directive.

signal, the inequality of load is greater than the discharge's one ($G_L/G_Q > 1$).

Our framework for estimating load flashiness can be compared to the bivariate plot of beta and the coefficient of variations ratio proposed by Musolff et al. (2015), based on the ratio of coefficient of variation of the concentration to discharge. Our load-flashiness diagram (**Figure 6C**) is based on b_{50high}—shown to be more selective in characterizing the export regimes between constituents (Underwood et al., 2017)—and presents a large dataset (over 1.5 million measurements). As a result, our load-flashiness diagram (**Figure 6C**) presents a larger dispersion, especially for chemodynamics export regimes. Moreover, proposing to replace the Musolff et al. (2015) export regime with W_2, a proxy more directly related to variation of discharge, will help determine the impact of hydrological change, such as those potentially induced by climate change on load exports. Flow flashiness (W_2) is a proxy of hydrological reactivity, which includes surficial and groundwater inputs. Deciphering between these different water sources could be assessed by examining patterns of their specific solute tracers as proposed by Li et al. (2017) and Zhi et al. (2019).

Optimizing Sampling Frequency for Reducing Load Calculation Uncertainty

Our results provide a water quality monitoring strategy that can address the large range of M2 values measured in our dataset for different solutes and catchments (**Figure 8**). We demonstrated

that relationship between uncertainties and loads flashiness M_2 combined with b_{50high}, can be used to calculate bias and precision for a given sampling frequency. Because sampling interval curves correspond to different $^{M}2^{\text{ values}}$ (e.g., **Figures 8**, **9** displayed results for a targeted uncertainty of 10%), these results can also be used to determine the optimal sampling frequency for a given uncertainty (Moatar et al., 2013). Uncertainties of the different load estimates may vary substantially, depending on the particular solute and particulate, differences in hydro-climate, and basin size. The method considers both the river-borne constituent considered and the hydrological characteristics of the catchments. Hence, sampling frequency should be adapted to each station and each solute or particulate, characterized by W_2 and b_{50high}, if a given regulatory uncertainty level is required. For instance, to characterize and manage eutrophication risks related to total phosphorus inputs from smaller catchments (medium flashiness class, chemodynamic behavior) to freshwater lakes requires more intensive sampling than nitrate inputs from larger catchments (low flashiness class, chemostatic behavior) that can stimulate coastal zone eutrophication. Yet, an adaptive sampling strategy is rarely achieved in existing surveys. In France, the national monitoring program, designed to fulfill the European Water Framework Directive, recommends a fixed monthly sampling frequency, whatever the water-borne material or the catchment size considered. Yet, our results (**Figure 9**) show that a 30 days sampling frequency is not appropriate to calculate loads with a reasonable uncertainty ($\pm 10\%$) in more than 90% of

TABLE 4 | Relationships between W_2, b_{50high}, and M_2 indicators and catchment characteristics: total percentage of variance explained by final regression models following a backward selection approach of explanatory variables (third column) and individual contributions (between 0 and 100%; next columns) of the selected variables according to hierarchical variation partitioning.

| | | Indicator/Constituent | | | | | | | | | | |
| | | W_2 | b_{50high} | | | | | M_2 | | | | |
	Units	–	TSS	TDS	TP	NO3	DOC	TSS	TDS	TP	NO3	DOC
% of explained variance	%	34.9	21.9	22.9	18.2	10.9	12.1	30.9	36.5	37.9	28.3	33.1
Area	km^2	**21.3**	9.6		15.5			12.9	**16.9**	7	10.8	**19**
Stream network density	km/km^2	**25.4**		11.7			20.6	**24.9**	**15.7**	**16.6**	**39.1**	**19.7**
Wetlands	%	7.3	**19**				**20.9**	1.4			6.8	13.5
Crystalline rocks	%		**44.1**	8	**30.9**	4.8	**41.3**	15.3	2.9		3.9	4.8
Low carbonate rocks	%	11.6		6.8		4		**27.8**	8.4	14.4		13.7
High carbonate rocks	%	5.1		12.7		5.6			4.5	2		
Riparian vegetation	%						4.6		5.8			
Forest	%	10.2			12.8	20.5		4.2			8.2	10.1
Extensive agriculture	%	2.6				**26.8**	3.7	2.8		3.2	3.3	3.3
Intensive agriculture	%	**13.6**		**18.5**	**27.1**			8.9	**31.1**	**33.9**	**14**	**15.9**
Urban area	%		17.2	**42.2**				1.7	10.9	5		
Population density	ind/km^2	3				11.2						
Point source P	kg/ha/yr				**22.8**					9.8		
Soil P	g/kg									8.1		
Point source N	kg/ha/yr										7.8	
N surplus	kgN/kg										6.2	
Erosion risk	%		10.2		17.9		8.9	3.8				

Blue and red cells indicate positive and negative relationships, respectively. Bold numbers highlight variables with the greatest influence (cumulated contribution >50%).

cases. Our approach to determine M_2, based on W_2 and b_{50high}, allows the determination of optimal sampling frequency, but also provides a measure of imprecision of past load measurements based on inadequate frequencies. Therefore, past load trends for the last 20–30 years can be recalculated, even based on classical monthly frequency. Based on these load trend recalculation, one can, for example, evaluate response-time of drainage basins to a given land use change and/or water policy implementation. Moreover, effects of potential hydrological changes (resulting in different W_2) based on climate change scenarios on loads, could be estimated with more accuracy.

Drainage Basin Characteristics as Predictor of M_2, b_{50high}, and W_2

Our study is the first to our knowledge that analyses the environmental factors controlling load variability (M_2). Although, the total explained variance is relatively low, i.e., 28–38% depending on the constituent (**Table 4**), one should emphasize that it represents the variance explained by an indicator of load variability. Indeed, trying to explain the variance of a variability is not an easy task, especially because our approach does not consider the temporal successions of climatic and hydrological events. Explained variance could likely be improved with other proxies, such topographic and hydroclimatic indicators. However, a still significant part of the variance of the studied solute flashiness (M_2) and its proxies, i.e., W_2 and b_{50high}, could be explained with a multi-variate model

of widely-available drainage basin characteristics, e.g., drainage basin size, percentage of intensive agriculture and percentage of stream network density (**Table 2**). Many studies since the 1970s have attempted to relate inter-annual means of solute concentrations and loads with drainage basin lithology, land cover and land use (Dupas et al., 2015). For instance, Omernik (1976) found a significant relationship between percentage of cropland in the drainage basin and nitrogen and phosphorus loads. Jones et al. (1976) reported a significant negative relationship between the percentage of wetlands in the drainage basin and nitrate loads—the very first large scale hint of the role of denitrification in wetland as a mechanism to buffer nitrate loads. In a large-scale study, Aitkenhead and McDowell (2000) calculated that mean soil C/N ratio of a biome accounted for 99.2% of the variance in annual riverine DOC concentrations. Yet, these large-scale relationships do not hold when analyzing smaller drainage basins, i.e., <few hundreds of km^2 often corresponding to the local water management scale, due to major influence of the spatial arrangements of land uses and the heterogeneity of geology and topography in solutes loads (Burt and Pinay, 2005; Abbott et al., 2018). Hence, the significant negative relationship between M_2 and drainage basin size, which stresses the need to focus more intensive monitoring on small catchments if we want to quantify catchment flashiness. Indeed, in small catchments lateral inputs of nutrients and carbon during high water period are often orders of magnitude higher than instream retention or removal (Brookshire et al., 2009). The

significant positive relationship between percentage of intensive agriculture and both load and flow flashiness (M_2 and W_2) agrees with the idea that a similar positive significant relationship occurs with water flashiness (W_2). Intensive agriculture practices often simplify the landscape, creating open fields, removing hedgerows, rectifying streams and draining soils (also positively related to flashiness, **Table 2**). All these practices contribute to increased runoff and to the reduction of solutes and particles retention. Hence, since a higher degree of water and transported constituents' flashiness is expected in intensive agriculture catchments, they require a more frequent monitoring design.

Differences in load flashiness among the various waterborne materials align with catchment variations in the sources and fate of those materials. For example, the positive relationship between DOC flashiness and the percentage of wetlands confirms their significant contribution to stream DOC (Zarnetske et al., 2018). The negative relationships between percentage of crystalline rocks or schist parent material on TSS, TP, and DOC export pattern, reveals a generally less intensive agricultural activity on these parent materials. This pattern may also be due to a dilution of these constituents by deep groundwater during high flow events (Thomas et al., 2016). It is worth noticing that nitrate exhibited a biogeochemical stationary behavior (*sensu* Basu et al., 2010), with b_{50high} mostly close to zero values. This result suggests a legacy storage of antecedent intensive fertilization (Aquilina et al., 2012; Van Meter et al., 2016), However, b_{50high} was significantly positively relate to the percentage of agriculture, which implies that during high water regime, nitrate stock mobilization in agricultural catchments can still increase with discharge increase. This finding underlines the necessity to tailor monitoring schemes to catchment characteristics. Although many nitrate monitoring schemes may warrant lower intensity in many situations, sampling intervals in agricultural catchments should be shortened, especially in the context of more frequent intense rainfall events under climate change.

CONCLUSION

We were able to demonstrate that load flashiness (M_2), i.e., percentage of cumulative load that occurs during the highest 2% of daily load values is a useful proxy of solute and sediment export regimes. Our results emerged from a robust, long-term dataset of a wide range of discharge, solute and particulate sediments in 580 drainage basins in France and the USA and 2,507 sample series, representing over 1.5 million discharge-concentration couples. This indicator can be estimated from the common low-frequency national or regional monitoring surveys through the b_{50high} coefficient and the runoff flashiness indicator (W_2). We showed that if current water-sampling strategies undertaken by local, national, and international water authorities are not appropriate to directly calculate solutes and sediment loads; these data can nevertheless be used to calculate flow flashiness (W_2) and b_{50high}. We demonstrated that these two proxies are related to load flashiness (M_2) with a simple equation. We showed that load flashiness diagrams can be used to classify constituents and catchments by precision related to different sampling intervals

and thus optimize stream water quality sampling procedures for a given transported constituent. Moreover, the analysis of our large dataset allowed the identification of significant correlations between easily accessible drainage basin characteristics (e.g., basin area, stream network density, and percentage of extensive agriculture), W_2, b_{50high}, and M_2. These characteristics can serve as a basis to classify non-monitored drainage basins as a function of their potential load flashiness and propose a sampling monitoring design for the most contributive ones. Regulatory monitoring in Europe, recommended by the WFD, promotes the monthly sampling for any monitored constituents (dissolved and particulate) and for any basin size. Such standardized monitoring does not take into account the actual variability of the constituent concentration and loads, particularly for the small (100–1,000 km^2) and very small (<100 km^2) basins. The load flashiness M_2 can also be used to optimize monitoring frequency to reach a certain level of annual load uncertainty (here 10%) for loads trend detection required for instance by international conventions such as OSPAR and HELCOM.

DATA AVAILABILITY STATEMENT

The datasets generated for this study are available on request to the corresponding author.

AUTHOR CONTRIBUTIONS

FUNDING

ACKNOWLEDGMENTS

SUPPLEMENTARY MATERIAL

The Supplementary Material for this article can be found online at: https://www.frontiersin.org/articles/10.3389/fevo.2019.00516/full#supplementary-material

Figure S1 | Predicted M_2 vs. observed M_2. **(A)** For French sites (TSS, TDS, TP, NO_3, DOC) and US (TSS and TDS) calibration set of data. **(B)** For streams of Lake Erie Region, data not used in the calibration procedure (TSS, TDS, TP, NO_3).

Figure S2 | Comparison analysis on 248 French stations of M_2 estimates derived from segmented linear regression approach (Method SRC_{50}) on monthly TSS, TP, and NO_3, and daily discharge vs. M_2 estimates derived from a Weighted Regression on Time Discharge and Seasonality (Method WRTDS, Q. Zhang pers. comm.).

Figure S3 | Temporal evolution of yearly b_{50high} estimated for TSS, TDS, TP, and NO_3 on five long-term and daily Lake Erie tributaries datasets.

Figure S4 | Temporal evolution of yearly M_2 and W_2 estimated for TSS, TDS, TP, and NO_3 on five long-term and daily Lake Erie tributaries datasets.

Table S1 | Error nomograph (e_{10}, e_{90} vs. M_2) for annual loads calculated for discharge-weighted concentration method. Lower limits ($e10$) and upper limits ($e90$) for sampling intervals of 3, 7,..., 60 days (Moatar et al., 2013).

Table S2 | Percentage of sites with significant p-values for segmented C-Q regressions. Total suspended solids (TSS), total dissolved solutes (TDS), total phosphorus (TP), nitrate (NO3), dissolve organic carbon (DOC).

REFERENCES

Abbott, B. W., Gruau, G., Zarnetske, J. P., Moatar, F., Barbe, L., Thomas, Z., et al. (2018). Unexpected spatial stability of water chemistry in headwater stream networks. *Ecol. Lett.* 21, 296–308. doi: 10.1111/ele.12897

Aitkenhead, J., and McDowell, W. H. (2000). Soil C: N ratio as a predictor of annual riverine DOC flux at local and global scales. *Glob. Biogeochem. Cycles* 14, 127–138. doi: 10.1029/1999GB900083

Aquilina, L., Vergnaud-Ayraud, V., Labasque, T., Bour, O., Molénat, J., Ruiz, L., et al. (2012). Nitrate dynamics in agricultural catchments deduced from groundwater dating and long-term nitrate monitoring in surface-and groundwaters. *Sci. Tot. Environ.* 435, 167–178. doi: 10.1016/j.scitotenv.2012.06.028

Basu, N. B., Destouni, G., Jawitz, J. W., Thompson, S. E., Loukinova, N. V., Darracq, A., et al. (2010). Nutrient loads exported from managed catchments reveal emergent biogeochemical stationarity. *Geophys. Res. Lett.* 37:L23404. doi: 10.1029/2010GL045168

Breitburg, D., Levin, L. A., Oschlies, A., Grégoire, M., Chavez, F. P., Conley, D. J., et al. (2018). Declining oxygen in the global ocean and coastal waters. *Science* 359:eaam7240. doi: 10.1126/science.aam7240

Brookshire, E., Valett, H., and Gerber, S. (2009). Maintenance of terrestrial nutrient loss signatures during in-stream transport. *Ecology* 90, 293–299. doi: 10.1890/08-0949.1

Burt, T., and Pinay, G. (2005). Linking hydrology and biogeochemistry in complex landscapes. *Prog. Phys. Geogr.* 29, 297–316. doi: 10.1191/0309133305pp450ra

Cerdan, O., Govers, G., Le Bissonnais, Y., Van Oost, K., Poesen, J., Saby, N., et al. (2010). Rates and spatial variations of soil erosion in Europe: a study based on erosion plot data. *Geomorphology* 122, 167–177. doi: 10.1016/j.geomorph.2010.06.011

Crowder, D., Demissie, M., and Markus, M. (2007). The accuracy of sediment loads when log-transformation produces nonlinear sediment load–discharge relationships. *J. Hydrol.* 336, 250–268. doi: 10.1016/j.jhydrol.2006.12.024

Delmas, M., Saby, N., Arrouays, D., Dupas, R., Lemercier, B., Pellerin, S., et al. (2015). Explaining and mapping total phosphorus content in French topsoils. *Soil Use Manage.* 31, 259–269. doi: 10.1111/sum.12192

Diamond, J. S., and Cohen, M. J. (2018). Complex patterns of catchment solute–discharge relationships for coastal plain rivers. *Hydrol. Process.* 32, 388–401. doi: 10.1002/hyp.11424

Dupas, R., Delmas, M., Dorioz, J. M., Garnier, J., Moatar, F., and Gascuel-Odoux, C. (2015). Assessing the impact of agricultural pressures on N and P loads and eutrophication risk. *Ecol. Indic.* 48, 396–407. doi: 10.1016/j.ecolind.2014.08.007

Ferguson, R. (1986). River loads underestimated by rating curves. *Water Resour. Res.* 22, 74–76. doi: 10.1029/WR022i001p00074

Frazar, S., Gold, A. J., Addy, K., Moatar, F., Birgand, F., Schroth, A. W., et al. (2019). Contrasting behavior of nitrate and phosphate flux from high flow events on small agricultural and urban watersheds. *Biogeochemistry* 145, 141–160. doi: 10.1007/s10533-019-00596-z

Gaillardet, J., Dupré, B., Louvat, P., and Allegre, C. (1999). Global silicate weathering and CO2 consumption rates deduced from the chemistry of large rivers. *Chem. Geol.* 159, 3–30. doi: 10.1016/S0009-2541(99)00031-5

Gall, H. E., Park, J., Harman, C. J., Jawitz, J. W., and Rao, P. S. C. (2013). Landscape filtering of hydrologic and biogeochemical responses in managed catchments. *Landsc. Ecol.* 28, 651–664. doi: 10.1007/s10980-012-9829-x

Godsey, S. E., Hartmann, J., and Kirchner, J. W. (2019). Catchment chemostasis revisited: water quality responds differently to variations in weather and climate. *Hydrol. Process.* 33, 3056–3069. doi: 10.1002/hyp.13554

Godsey, S. E., Kirchner, J. W., and Clow, D. W. (2009). Concentration–discharge relationships reflect chemostatic characteristics of US catchments. *Hydrol. Process.* 23, 1844–1864. doi: 10.1002/hyp.7315

Hirsch, R. M., Moyer, D. L., and Archfield, S. A. (2010). Weighted regressions on time, discharge, and season (WRTDS), with an application to Chesapeake Bay river inputs 1. *J. Am. Water Resour. Assoc.* 46, 857–880. doi: 10.1111/j.1752-1688.2010.00482.x

Jarvie, H. P., Smith, D. R., Norton, L. R., Edwards, F. K., Bowes, M. J., King, S. M., et al. (2018). Phosphorus and nitrogen limitation and impairment of headwater streams relative to rivers in Great Britain: a national perspective on eutrophication. *Sci. Tot. Environ.* 621, 849–862. doi: 10.1016/j.scitotenv.2017.11.128

Jawitz, J. W., and Mitchell, J. (2011). Temporal inequality in catchment discharge and solute export. *Water Resour. Res.* 47:W00J14. doi: 10.1029/2010WR010197

Johnes, P. J. (2007). Uncertainties in annual riverine phosphorus load estimation: impact of load estimation methodology, sampling frequency, baseflow index and catchment population density. *J. Hydrol.* 332, 241–258. doi: 10.1016/j.jhydrol.2006.07.006

Jones, J., Borofka, B., and Bachmann, R. (1976). Factors affecting nutrient loads in some Iowa streams. *Water Res.* 10, 117–122. doi: 10.1016/0043-1354(76)90109-3

Le Moal, M., Gascuel-Odoux, C., Ménesguen, A., Souchon, Y., Étrillard, C., Levain, A. et al. (2019). Eutrophication: a new wine in an old bottle? *Sci. Tot. Environ.* 651, 1–11. doi: 10.1016/j.scitotenv.2018.09.139

Lee, C. J., Hirsch, R. M., Schwarz, G. E., Holtschlag, D. J., Preston, S. D., Crawford, C. G., et al. (2016). An evaluation of methods for estimating decadal stream loads. *J. Hydrol.* 542, 185–203. doi: 10.1016/j.jhydrol.2016.08.059

Li, L., Bao, C., Sullivan, P. L., Brantley, S., Shi, Y., and Duffy, C. (2017). Understanding watershed hydrogeochemistry: 2. Synchronized hydrological and geochemical processes drive stream chemostatic behavior. *Water Resour. Res.* 53, 2346–2367. doi: 10.1002/2016WR018935

Littlewood, I. G., and Marsh, T. J. (2005). Annual freshwater river mass loads from Great Britain, 1975-1994: estimation algorithm, database and monitoring network issues. *J. Hydrol.* 304, 221–237. doi: 10.1016/j.jhydrol.2004.07.031

Meybeck, M. (1987). Global chemical weathering of surficial rocks estimated from river dissolved loads. *Am. J. Sci.* 287, 401–428. doi: 10.2475/ajs.287.5.401

Meybeck, M., and Helmer, R. (1989). The quality of rivers: from pristine stage to global pollution. *Palaeogeogr. Palaeoclimatol. Palaeoecol.* 75, 283–309. doi: 10.1016/0031-0182(89)90191-0

Meybeck, M., Laroche, L., Dürr, H., and Syvitski, J. (2003). Global variability of daily total suspended solids and their fluxes in rivers. *Glob. Planet. Change* 39, 65–93. doi: 10.1016/S0921-8181(03)00018-3

Meybeck, M., and Moatar, F. (2012). Daily variability of river concentrations and fluxes: indicators based on the segmentation of the rating curve. *Hydrol. Process.* 26, 1188–1207. doi: 10.1002/hyp.8211

Minaudo, C., Dupas, R., Gascuel-Odoux, C., Fovet, O., Mellander, P. E., Jordan, P., et al. (2017). Nonlinear empirical modeling to estimate phosphorus exports using continuous records of turbidity and discharge. *Water Resour. Res.* 53, 7590–7606. doi: 10.1002/2017WR020590

Minaudo, C., Dupas, R., Gascuel-Odoux, C., Roubeix, V., Danis, P.-A., and Moatar, F. (2019). Seasonal and event-based concentration-discharge relationships to identify catchment controls on nutrient export regimes. *Adv. Water Resour.* 131:103379. doi: 10.1016/j.advwatres.2019.103379

Moatar, F., Abbott, B. W., Minaudo, C., Curie, F., and Pinay, G. (2017). Elemental properties, hydrology, and biology interact to shape concentration-discharge

curves for carbon, nutrients, sediment, and major ions. *Water Resour. Res.* 53, 1270–1287. doi: 10.1002/2016WR019635

Moatar, F., and Meybeck, M. (2005). Compared performances of different algorithms for estimating annual nutrient loads discharged by the eutrophic River Loire. *Hydrol. Process.* 19, 429–444. doi: 10.1002/hyp.5541

Moatar, F., and Meybeck, M. (2007). Riverine fluxes of pollutants: towards predictions of uncertainties by flux duration indicators. *Comptes Rendus Geosci.* 339, 367–382. doi: 10.1016/j.crte.2007.05.001

Moatar, F., Meybeck, M., Raymond, S., Birgand, F., and Curie, F. (2013). River flux uncertainties predicted by hydrological variability and riverine material behaviour. *Hydrol. Process.* 27, 3535–3546. doi: 10.1002/hyp.9464

Musolff, A., Fleckenstein, J., Rao, P., and Jawitz, J. (2017). Emergent archetype patterns of coupled hydrologic and biogeochemical responses in catchments. *Geophys. Res. Lett.* 44, 4143–4151. doi: 10.1002/2017GL072630

Musolff, A., Schmidt, C., Selle, B., and Fleckenstein, J. H. (2015). Catchment controls on solute export. *Adv. Water Resour.* 86, 133–146. doi: 10.1016/j.advwatres.2015.09.026

Nemery, J., Mano, V., Coynel, A., Etcheber, H., Moatar, F., Meybeck, M., et al. (2013). Carbon and suspended sediment transport in an impounded alpine river (Isere, France). *Hydrol. Process.* 27, 2498–2508. doi: 10.1002/hyp.9387

Omernik, J. M. (1976). *The Influence of Land Use on Stream Nutrient Levels, Vol. 76.* US Environmental Protection Agency; Office of Research and Development; Corvallis Environmental Research Laboratory; Eutrophication Survey Branch.

Oudin, L., Andréassian, V., Perrin, C., Michel, C., and Le Moine, N. (2008). Spatial proximity, physical similarity, regression and ungaged catchments: a comparison of regionalization approaches based on 913 French catchments. *Water Resour. Res.* 44:W03413. doi: 10.1029/2007WR006240

Quinn, P. F., Beven, K. J., and Lamb, R. (1995). The Ln(A/tanβ) index – How to calculate it and how to use it withing the Topmodel framework. *Hydrol. Process.* 9, 161–182.

Raymond, P. A., and Saiers, J. E. (2010). Event controlled DOC export from forested watersheds. *Biogeochemistry* 100, 197–209. doi: 10.1007/s10533-010-9416-7

Raymond, S., Moatar, F., Meybeck, M., and Bustillo, V. (2013). Choosing methods for estimating dissolved and particulate riverine fluxes from monthly sampling. *Hydrol. Sci. J.* 58, 1326–1339. doi: 10.1080/02626667.2013.814915

Scheffer, M., Bascompte, J., Brock, W. A., Brovkin, V., Carpenter, S. R., Dakos, V., et al. (2009). Early-warning signals for critical transitions. *Nature* 461:53. doi: 10.1038/nature08227

Schoumans, O. F., Silgram, M., Groenendijk, P., Bouraoui, F., Andersen, H. E., Kronvang, B., et al. (2009). Description of nine nutrient loss models: capabilities and suitability based on their characteristics. *J. Environ. Monit.* 11, 506–514. doi: 10.1039/b823239c

Skeffington, R. A., Halliday, S. J., Wade, A. J., Bowes, M. J., and Loewenthal, M. (2015). Using high-frequency water quality data to assess sampling strategies for the EU Water Framework Directive. *Hydrol. Earth Syst. Sci.* 19, 2491–2504. doi: 10.5194/hess-19-2491-2015

Syvitski, J. P., and Morehead, M. D. (1999). Estimating river-sediment discharge to the ocean: application to the Eel margin, northern California. *Mar. Geol.* 154, 13–28. doi: 10.1016/S0025-3227(98)00100-5

Thomas, Z., Abbott, B., Troccaz, O., Baudry, J., and Pinay, G. (2016). Proximate and ultimate controls on carbon and nutrient dynamics of small agricultural catchments. *Biogeosciences* 13, 1863–1875. doi: 10.5194/bg-13-1863-2016

Underwood, K. L., Rizzo, D. M., Schroth, A. W., and Dewoolkar, M. M. (2017). Evaluating spatial variability in sediment and phosphorus concentration-discharge relationships using Bayesian inference and self-organizing maps. *Water Resour. Res.* 53, 10293–10316. doi: 10.1002/2017WR021353

Van Meter, K., Basu, N., and Van Cappellen, P. (2017). Two centuries of nitrogen dynamics: legacy sources and sinks in the Mississippi and Susquehanna River Basins. *Glob. Biogeochem. Cycles* 31, 2–23. doi: 10.1002/2016GB005498

Van Meter, K. J., Basu, N. B., Veenstra, J. J., and Burras, C. L. (2016). The nitrogen legacy: emerging evidence of nitrogen accumulation in anthropogenic landscapes. *Environ. Res. Lett.* 11:035014. doi: 10.1088/1748-9326/11/3/035014

Vanmaercke, M., Poesen, J., Verstraeten, G., de Vente, J., and Ocakoglu, F. (2011). Sediment yield in Europe: spatial patterns and scale dependency. *Geomorphology* 130, 142–161. doi: 10.1016/j.geomorph.2011.03.010

Walsh, C., and Mac Nally, R. (2013) *hier.part: Hierarchical Partitioning.* R package version 1.0-4. Vienna: R Foundation for Statistical Computing. Available online at: http://CRAN.R-project.org/package=hier.part (accessed September 15, 2019).

Yoon, B., and Raymond, P. A. (2012). Dissolved organic matter export from a forested watershed during Hurricane Irene. *Geophys. Res. Lett.* 39:L18402. doi: 10.1029/2012GL052785

Zarnetske, J. P., Bouda, M., Abbott, B. W., Saiers, J., and Raymond, P. A. (2018). Generality of hydrologic transport limitation of watershed organic carbon flux across ecoregions of the United States. *Geophys. Res. Lett.* 45, 702–711. doi: 10.1029/2018GL080005

Zhang, Q. (2018). Synthesis of nutrient and sediment export patterns in the Chesapeake Bay watershed: complex and non-stationary concentration-discharge relationships. *Sci. Tot. Environ.* 618, 1268–1283. doi: 10.1016/j.scitotenv.2017.09.221

Zhang, Q., Blomquist, J. B., Moyer, D. L., and Chanat, J. G. (2019). Estimation bias in water-quality constituent concentrations and fluxes: a synthesis for chesapeake bay rivers and streams. *Front. Ecol. Evol.* 7:109. doi: 10.3389/fevo.2019.00109

Zhi, W., Li, L., Dong, W., Brown, W., Kaye, J., Steefel, C., et al. (2019). Distinct source water chemistry shapes contrasting concentration-discharge patterns. *Water Resour. Res.* 55, 4233–4251. doi: 10.1029/2018WR024257

APPENDIX

Deriving Mp From Daily Discharge and Concentration-Discharge Relations

Assume that the distribution of daily flows Q is lognormal with parameters μ and σ^2, i.e., $\log(Q) \sim N(\mu, \sigma^2)$. For a lognormal distribution, Jawitz and Mitchell (2011) show that the Lorenz curve is equal to:

$$Yp = \phi\left(\phi^{-1}(p\%) - \sigma\right) \qquad (A1)$$

where ϕ is the standard normal cdf and ϕ^{-1} its inverse (also known as the probit transformation).

Since the Lorenz curve Yp and the flow flashiness Wp are related through the relation $W_p = 1 - Y_{1-p}$, flow flashiness is equal to:

$$Wp = 1 - \phi\left(\phi^{-1}(1 - p\%) - \sigma\right) \qquad (A2)$$

Moreover, assume that the daily log-concentration $\log(C)$ can be derived from daily flows as follows:

$$\log(C) = a + b.\log(Q) + \varepsilon; \ \varepsilon \sim N(0, \eta^2) \qquad (A3)$$

Daily log-loads can therefore be computed as follows:

$$\begin{aligned}\log(L) = \ & \log(CQ) = \log(C) + log(Q) = a \\ & + (b+1).\log(Q) + \varepsilon; \ \varepsilon \sim N(0, \eta^2)\end{aligned} \qquad (A4)$$

This equation implies that daily loads L follow a lognormal

distribution with mean $a + (b+1).\mu$ and variance $(b+1)^2 \sigma^2 + \eta^2$. Consequently, load flashiness is equal to:

$$Mp = 1 - \phi\left(\phi^{-1}(1 - p\%) - \sqrt{(b+1)^2 \sigma^2 + \eta^2}\right) \qquad (A5)$$

Some additional algebra [using the relation $\phi^{-1}(1 - u) = -\phi^{-1}(u)$] leads to the following relation between flow and load flashiness:

$$\phi^{-1}(Mp) = \phi^{-1}(Wp) + \sigma\left(\sqrt{(b+1)^2 + \left(\frac{\eta}{\sigma}\right)^2} - 1\right) \qquad (A6)$$

When the quality of the concentration-discharge regression is good ($\eta \ll \sigma$), this relation simplifies to:

$$\phi^{-1}(Mp) = \phi^{-1}(Wp) + \sigma b$$

Note that the formula above are given for one particular catchment i and constituent j. Making the catchment and element indices explicit is useful to distinguish quantities that vary across catchments only or across catchments and constituents:

$$\phi^{-1}(Mp_{i,j}) = \phi^{-1}(Wp_i) + \sigma_i\left(\sqrt{(b_{i,j}+1) + \left(\frac{\eta_{i,j}}{\sigma_i}\right)^2} - 1\right) \qquad (A7)$$

$$\text{Simplified version}: \phi^{-1}(Mp_{i,j}) = \phi^{-1}(Wp_i) + \sigma_i b_{i,j} \qquad (A8)$$